

# A phenomenological model of magnetic flux tubes in strong fields induced by axion-origin photons

Vitaliy D. Rusov\* and Tatyana N. Zelentsova

*Department of Theoretical and Experimental Nuclear Physics,  
Odessa Polytechnic National University,  
1 Shevchenko ave., Odessa 65044, Ukraine*

(Dated: March 17, 2026)

We propose a phenomenological model in which empty flux tubes in strong magnetic fields are associated with both the conversion of axions to photons of axion origin to generate coronal heating, and the simultaneous preservation of the Parker-Biermann cooling effect by converting high-energy photons from the radiative zone to axions from the convective zone through the O-loop tachocline, is the source of the rise of the magnetic flux tube from the tachocline to the photosphere in the form of sunspots.

The model is characterized by two free parameters, justified by existing theoretical and observational constraints, the axion mass  $m_a \sim 3.2 \cdot 10^{-2} \text{ eV}$ , and asymmetric dark matter (ADM) with a particle mass  $m_{ADM} \sim 5 \text{ GeV}$  gravitationally captured by the Sun. In this scenario, temporal modulations of the axion density are caused by anticorrelated 11-year modulations of ADM gravitationally captured by the Sun.

We also obtained theoretical estimates of the velocities and times in empty magnetic tubes in strong fields rising from the tachocline to the surface of the photosphere in the form of sunspots. This ensured complete agreement with known experimentally measured velocities and times using local helioseismological time-distance inversions along the ray trajectories of acoustic waves. This allows us to study not only the subsurface structure and dynamics of active regions, but also the depths of the empty magnetic flux tube, extending up to 200,000 km from the tachocline to the photosphere.

The proposed model links the phenomenology of axions with the magnetic structures of the Sun and provides testable consequences for astrophysical and solar observations.

## I. INTRODUCTION

It is well known that helioseismological methods are well-suited for studying the Sun's rotation and structure from helioseismic reversals, but they have difficulty distinguishing the effects of very strong magnetic fields from other structural changes, and therefore cannot definitively confirm the presence of a magnetic field in the solar tachocline exceeding  $10^5 \text{ G}$ . In other words, it is difficult to distinguish the effects of very strong magnetic fields in the tachocline, but this does not mean they should be discarded due to their virtually undetectable nature using direct seismic methods.

This raises the question of why the dynamo action is only associated with a magnetic field of about  $10^5 \text{ G}$ , but is definitely not associated with a stronger magnetic field of about  $10^7 \text{ G}$ ? It is known that "...even if complete knowledge of the solar dynamo existed – and it does not...", as has been pointed out throughout the review [1] – a number of crucial questions require answers, including, at least: How do sunspots with structure, rotation velocity, and 11-year luminosity form and disappear? Why has spot formation not been captured even in local models, let alone global models? How do turbulence coefficients – turbulent pumping, turbulent diffusion – change with rotation velocity, luminosity, and in-

ternal structure? Why the inability to model accurately enough the surface layers where the density drops vertiginously is, according to [2], the common characteristic of all existing dynamo models? At that, using the so-called new era of 3D modeling and observations [1], they (solar physicists), surprisingly, believe that the study of the solar dynamo will be definitely solved within the next 10-20 years.

But the most important thing is that any dynamo action that involves, for example, the 11-year oscillations of sunspots or a sunspot butterfly diagram, must contain a small number of "free parameters" – usually three or less (see Dahlquist's key theorem [3]) – because of the mathematical structure of the problem, where the independence of the equations, the stability of the system, and the dimensionality restrictions reduce the number of "degrees of freedom" needed to determine the solution.

We could raise a few more questions, but it is enough for us that "...not enough for a scientific understanding of the solar dynamo. For there is an unfortunate revelation: with four free parameters you can provide a satisfactory fit to the horizon of New York or Beijing" – as was said by the great Eugene N. Parker, who in 2009 in his last article [4] first began to strongly doubt the existence of the solar dynamo.

Now, in contrast to the no more than of three "free" parameters of the solar dynamo, consider our next two "free" parameters: the dark matter axions in the Sun's core and the dark matter asymmetry (ADM) gravitationally captured by the Sun. These variables in the corre-

---

\* Corresponding author e-mail: [siis@te.net.ua](mailto:siis@te.net.ua)

sponding models cannot be predicted by the theory itself and must be determined from experimental data, as they are related to fundamental physical constants.

Let us first consider the first “free parameter” – the dark matter axions in the Sun’s core, which are necessary to solve the well-known problem of energy transfer by magnetic flux tubes from the tachocline to the Sun’s photosphere.

It is known that the unsolved problem of energy transport by magnetic flux tubes at the same time represents another unsolved problem related to the sunspot darkness (see 2.2 in [5]). Of all the known concepts playing a noticeable role in understanding the connection between the energy transport and sunspot darkness, let us consider the most significant theory, in our view. It is based on the Parker-Biermann cooling effect [6–8] and originates from the early works of Biermann [7] and Alfvén [9].

As you know, the Parker-Biermann cooling effect [6–8], which plays a role in our current understanding, originates from Biermann [7] and Alfvén [9]: in a highly ionized plasma, the electrical conductivity can be so large that the magnetic fields are frozen into the plasma. Biermann realized that the magnetic field in the spots themselves can be the cause of their coolness – it is colder because the magnetic field suppresses the convective heat transport. Hence, the darkness of the spot is due to a decrease in surface brightness.

Parker [6, 8, 10–12] pointed out that the magnetic field can be compressed to the enormous intensity only by reducing the gas pressure within the flux tube relative to the pressure outside, so that the external pressure compresses the field. The only known mechanism for reducing the internal pressure sufficiently is a reduction of the internal temperature over several scale heights so that the gravitational field of the Sun pulls the gas down out of the tube (as described by the known barometric law  $dp/dz = -\rho g$ ). Hence it appears that the intense magnetic field of the sunspot is a direct consequence of the observed reduced temperature [6].

On the other hand, Parker [12, 13] has also pointed out that the magnetic inhibition of convective heat transport beneath the sunspot, with the associated heat accumulation below, raises the temperature in the lower part of the field. The barometric equilibrium leads to enhanced gas pressure upward along the magnetic field, causing the field to disperse rather than intensify. Consequently, [12] argued that the temperature of the gas must be influenced by something more than the inhibition of heat transport!

Our idea is that the explanation of sunspots is based not only on the suppression of convective heat transfer by a strong magnetic field (of the order of  $\sim 10^7 G$  [14]) through the enhanced cooling of the Parker-Biermann effect [10], but also on the appearance of the axions of photonic origin (Fig 2, Fig. B.1 in [14]) from the tachocline to the photosphere, which is confirmed by the “disappearance” of the heat, and consequently, the temperature in the lower part of the magnetic tube [12, 13] due to the ax-

ions of photonic origin from the photon-axion oscillations in the O-loop near the tachocline (see Fig. 2).

This means that the appearance of axions of photonic origin, with which the problem of temperature increase in the lower part of a strong magnetic tube disappears, and the photons of axionic origin, which have the free path (Rosseland length; see Fig. B.3 in [14]) from the tachocline to the photosphere, are the explanation of sunspots based not only on the suppression of convective heat transport by a strong magnetic field [14], but also on the indispensable existence of the Parker-Biermann cooling effect. At the same time, we clearly understand that stronger fields (e.g. of the order of  $10^7 G$ ) would seriously suppress the action of the dynamo (see [15]).

On the other hand, we understand that the existence of the Parker-Biermann cooling effect is associated with the so-called thermomagnetic Etingshausen-Nernst effect (see Appendix A in [14]). Due to the large temperature gradient in the tachocline, the thermomagnetic EN effect [16–19] creates electric currents that are inversely proportional to the strong magnetic field of the tachocline. It means that, using the thermomagnetic EN effect, a simple estimate of the magnetic pressure of an ideal gas in the tachocline of e.g. the Sun,

$$\frac{B_{tachoc}^2}{8\pi} = p_{ext} \approx 6.5 \cdot 10^{13} \frac{erg}{cm^3} \text{ at } 0.7R_{Sun}, \quad (1)$$

can indirectly prove that toroidal magnetic field of the tachocline is exactly equal to

$$B_{tachoc}^{Sun} = 4.1 \cdot 10^7 G, \quad (2)$$

Using the strong MFT field, we are interested in the existence of dark matter axions identical to solar axions, which strongly affects the conversion of axion origin photons in magnetic O-loops near the tachocline, and are thus related to the so-called thermomagnetic Etingshausen-Nernst effect through the Parker-Biermann cooling effect (see Appendix A in [14]). In order to answer this question, let us first consider all the unexpected and intriguing implications of the 11-year modulations of the ADM density in the solar interior and around the BH (see Sect. 3 in [14]).

It is well known that virtually all physicists, and astrophysicists in particular, know that asymmetric dark matter (ADM) exists in the Universe, and of course, in our galaxy, with the highest density of ADM located precisely at the galactic center, i.e. near the black hole. At the same time, we know that the periods, velocities, and modulations of the S-stars are the essential indicator of the modulation of the ADM halo density in the fundamental plane of the Galaxy’s center. Surprisingly, between the black hole and the disk, there are also so-called amazing S-stars [20], of which there are just over 30. Most intriguingly, the closest S-star to the black hole is called S-102, whose orbital period around the black hole

is 11 years (see Fig. 6 and Fig. 8 in [14]). From this we understand that when the S-102 passes very close to the black hole, the high speed of this star is such that dark matter is practically not captured by this star. But when the star S-102 orbits farther from the black hole, the star gravitationally captures these ADMs. If the modulations of the ADM halo at the GC lead to modulations of the ADM density on the surface of the Sun (through vertical density waves from the disk to the solar neighborhood), then there is an "experimental" anticorrelation identity between such indicators as the ADM density modulation in the solar interior and the sunspot cycles. Or equivalently, between the modulation of solar axions (or photons of axion origin) and the sunspot cycles!

A hypothetical pseudoscalar particle called axion is predicted by the theory related to solving the CP-invariance violation problem in QCD. The most important parameter determining the axion properties is the energy scale  $f_a$  of the so-called U(1) Peccei-Quinn symmetry violation. It determines both the axion mass and the strength of its coupling to fermions and gauge bosons including photons. However, in spite of the numerous direct experiments, axions have not been discovered so far. Meanwhile, these experiments together with the astrophysical and cosmological limitations leave a rather narrow band for the permissible parameters of invisible axion (e.g.  $10^{-6}eV \leq m_a \leq 10^{-2}eV$  (see [21, 22]; Fig. 13 in [23], Fig. 24 in [24])). The PQ mechanism, solving the strong CP problem in a very elegant way [25–28], is especially attractive here, since the axion is also a candidate for dark matter [29–31].

At present, we have shown that axions born in the core of the Sun, and photons of axion origin (in the million-degree solar corona) yield a tight constraint on the axion-photon coupling constant  $g_{a\gamma} \sim 4.4 \cdot 10^{-11} GeV^{-1}$  and mass  $m_a \sim 3.2 \cdot 10^{-2} eV$  (see Fig. 1a; also Fig.1 in [14]). Most importantly, hadronic axions produced in the solar core are controlled by anticorrelated 11-year variations in the density of asymmetric dark matter (ADM) gravitationally trapped in the solar interior (via vertical density waves from the black hole disk to the solar neighborhood), with the hard part of the solar photon spectrum being of axion origin, which is defined as the product of the axions fraction in the solar core and the fraction of the sunspot area. The latter is the result of solar luminosity variations (see Eqs. (27)-(28) in [14]). This means that solar luminosity variations and other solar cycles are the result of 11-year variations in ADM density, which are anticorrelated with the density of hadronic axions in the solar core.

Interestingly, in contrast to our Fig. 1a, in Fig. 1b, we can see a well-known strong constraint on the axion-photon coupling  $g_{a\gamma} \sim 4.4 \cdot 10^{-11} GeV^{-1}$ , but in a wide mass range (see Fig. 1b and Eq. (2) in [32]) from an analysis of a sample of 39 Galactic Globular Clusters. However, in our case (Fig. 1a) the wide range of masses [32] is, oddly enough, replaced by a single mass  $m_a \sim 3.2 \cdot 10^{-2} eV$ , which fits not only the axions of galac-

tic globular clusters [32], but also all axion stars in our galaxy, including neutron stars [33], supernovae [34, 35], and the Sun [14].

Taking into account the above, we structure our paper as follows. In Section II, we discuss the physics of nearly empty flux tubes and the connection with dark matter axions out of the solar core. In Section II A, we present convective heating and magnetic buoyancy of flux tubes by means of axion origin photons. In Section II B, we discuss the physics of primary and secondary reconnection of flux tubes in the lower layers and the features of the Joy's law tilt angle. In Section II B 2, we discuss the physics of the observed double maxima of sunspot cycles, where the first maximum does not depend on the tilt angle of the Joy's law, while the second one definitely depends on the tilt angle of the Joy's law. We also showed the relationship between the ADM density in the solar interior (or, for example, the number of anticorrelated sunspots) and the Gnevyshv gap. Finally, in Section III, we provide a summary and outlook for this paper.

## II. PHYSICS OF THE THEORY OF PRACTICALLY EMPTY FLUX TUBES IN STRONG FIELDS OF THE ORDER $\sim 10^7 G$

Of all the known concepts that play a significant role in understanding the connection between the energy transfer of a magnetic flux tube and the darkness of sunspots, we will consider what we believe to be the most significant. It is based on the Parker-Biermann cooling effect [6–8] in strong magnetic fields, which explains how the result of the suppression of Parker's convective heat transfer manifests itself in the lower part of the magnetic flux tube (see Fig. 2).

To understand the physics of the Parker's suppression of the convective heat transfer in strong magnetic fields, we need to turn to the dark matter axions originating from the Sun's core. Taking into account solar axions and the existence of a magnetic O-loop within the magnetic field near the tachocline (see Fig. 3d), the answer becomes very simple. When a magnetic O-loop forms within the magnetic field near the tachocline via a turbulent Kolmogorov cascade (see Fig. 3), dark matter axions and high-energy photons from the radiation zone to the tachocline undergo both axion-photon and photon-axion oscillations in this O-loop during the magnetic field in the tachocline, during which so-called of axion origin photons and photon origin axions emerge under a sunspot. This means that the Parker-Birman cooling effect exists due to the disappearance of barometric equilibrium [10, 11] and, as a consequence, the manifestation of the photon mean free path (Rosseland length; see Fig. B.3 in [14]) from the tachocline to the photosphere, which is confirmed by the existence of both axion-photon oscillations during the formation of axion origin photons, and simultaneously by the existence of photon-axion oscillations during the formation of photon origin axions during MTF

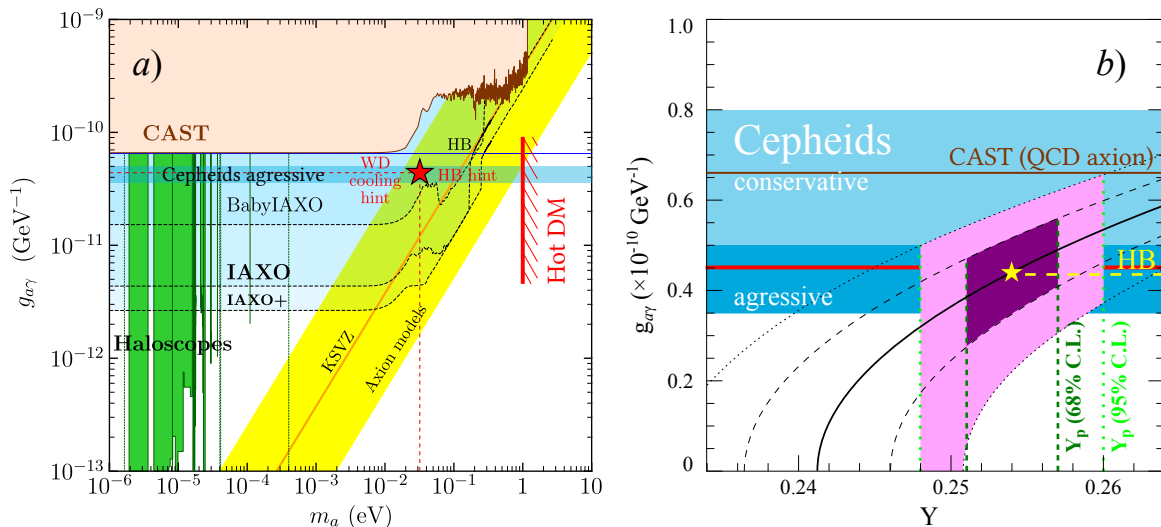


FIG. 1. (a) Summary of astrophysical, cosmological and laboratory constraints on axions. Comprehensive axion parameter space, highlighting two main front lines of direct detection experiments: helioscopes (CAST [36]) and haloscopes (ADMX [37], and RBF [38] and microwave resonators [39–43]). The astrophysical bounds from horizontal branch and massive stars are labeled “HB” [44] and “Cepheids” [45], respectively, and there are also astrophysical hints (WD cooling hints, and HB hint). The QCD motivated models (KSVZ [46, 47]) for axions lay in the yellow diagonal band. A plot of  $g_{a\gamma}$  versus  $m_a$  with the most stringent results (solid lines) and sensitivity perspectives (dashed lines) of observations and experiments directly comparable to the different phases of IAXO are shown, BabyIAXO, IAXO, and an upgraded version of IAXO, IAXO+. The yellow band denotes the region of the parameter space favoured by QCD axion models. The red star marks the values of the axion mass  $m_a \sim 3.2 \cdot 10^{-2} \text{ eV}$  and the axion-photon coupling constant  $g_{a\gamma} \sim 4.4 \cdot 10^{-11} \text{ GeV}^{-1}$ , which were first obtained experimentally (see [14]). (b)  $R$  parameter constraints, which compares the numbers of stars in the the horizontal branch (HB) and in the upper portion of the red giant branch (RGB), to helium mass fraction  $Y$  and axion coupling  $g_{a\gamma}$  (adopted from [32]). The resulting bound on the axion ( $g_{10} = g_{a\gamma}/(10^{-10} \text{ GeV}^{-1})$ ) is somewhere between rather conservative  $0.5 < g_{10} < 0.8$  and most aggressive  $0.35 < g_{10} < 0.5$  [48]. The red line marks the value of the axion–photon coupling constant  $g_{a\gamma} \sim 4.5 \cdot 10^{-11} \text{ GeV}^{-1}$  adopted from Eq. (2) in [32]. The blue shaded area represents the bounds from Cepheids observation. The yellow star corresponds to  $Y = 0.254$  and the bounds from HB lifetime (yellow dashed line).

in the tachocline (see Fig. 2).

On the other hand, high-energy photon fluxes coming from the radiation zone through the thin “ring” part of the magnetic tube, i.e. between the tachocline and the “ring” (or more precisely between the magnetic wall and the O-loop of the tube; see Figs. 2 and 3), and which is applied without the Parker-Biermann cooling effect, allows to determine the convective heating  $(dQ/dt)_2$  (see Sect. II A).

This solution clearly depends on the lifetime of the magnetic tubes rising from the tachocline to the surface of the Sun. That’s why due to the primary magnetic reconnection in the lower layers of the flux tubes (see Fig. 3d) this is not the final stage of the simulation. The essence of a practically empty tube in strong fields of  $\sim 10^7 \text{ G}$ , which is born for the first time without a dynamo of any type (see Fig. 4a), is associated with the physics of turbulent reconnection of magnetic bipolar structures (see Fig. 4b,c). It is very important that this is due to the topological effects of secondary magnetic reconnection in the lower layers of the magnetic tube. From here, the bipolar part of the  $\Omega$ -loop rearranges itself at its base, compressing the  $\Omega$ -loop (blue lines; see

Fig. 4b,c) and, as a consequence, organize a free O-loop (blue lines; Fig. 4d).

As described by [52–54], the upward convection flow around the rising  $\Omega$ -loop brings its “legs” together in such a way that the magnetic field reconnection occurs across this loop. This cuts off the magnetic loop from the azimuthal magnetic field, turning it into an O-loop (see Fig. 4 in [52] and Fig. 3 in [53]). After that the azimuthal magnetic field restores its initial configuration and becomes ready for another process with  $\Omega$ -loop.

Let us now make some important remarks on the turbulent reconnection, the  $\Omega$ -loop transformation into the O-loop by rapid “legs” closure, the restoration of the initial azimuthal field and the preconditions for another  $\Omega$ -loop formation in the same place. It is also necessary to explain the physical interpretation of the overshoot process near the tachocline and estimate the velocity  $v_{rise}$  and time  $\tau_d$  of the magnetic tube rise from the overshoot boundary layer – starting with the azimuthal magnetic flux strength of  $B_{tacho} \sim 4 \cdot 10^7 \text{ G}$  (see Eq. A.1 in [14]).

One of the final goals of this section is to determine the general regularities of the theory of magnetic flux tubes in strong fields of the order of  $\sim 10^7 \text{ G}$  using photons of

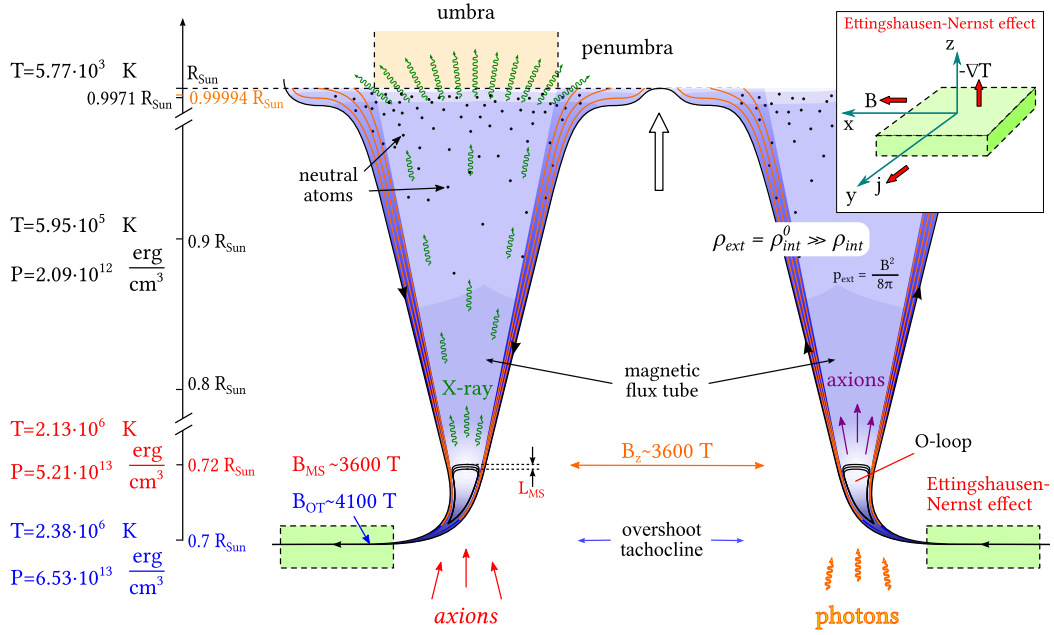


FIG. 2. Topological effects of magnetic reconnection inside the magnetic tubes with the “magnetic steps” (Fig. B.1 in [14]). The left panel shows the temperature and pressure change along the radius of the Sun from the tachocline to the photosphere [49],  $L_{MS}$  is the height of the magnetic shear steps. At  $R \sim 0.72 R_{\text{Sun}}$  the vertical magnetic field, which is developed from the horizontal part of the magnetic field (step) with the participation of the O-loop through the well-known Kolmogorov turbulent cascade (see Fig. 3), reaches  $B_z \sim 3600 \text{ T}$ , and the magnetic pressure  $p_{\text{ext}} = B^2/8\pi \simeq 5.21 \cdot 10^{13} \text{ erg/cm}^3$  [49]. The very cool regions along the entire convective zone caused by the Parker-Biermann cooling effect have the virtually zero internal gas pressure, i.e. the maximum magnetic pressure in the magnetic tubes. The narrow “purple” rings between the O-loop and the tube walls ( $\rho_{\text{ext}} = \rho_{\text{int}}^0 \gg \rho_{\text{int}}$ ) with the Parker-Bierman cooling effect inside, are a very important result of the existence of convective heating  $(dQ/dt)_2$  in Section II A.

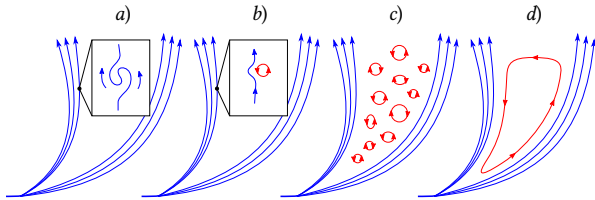


FIG. 3. Kolmogorov turbulent cascade [50, 51] and primary magnetic reconnection (which differs sharply from the secondary (see Fig. 4) in the lower layers inside the unipolar magnetic tube (Fig. B.2 in [14]). Common to these various turbulent systems is the presence of the Kolmogorov’s inertial region, through which the energy is cascaded from large to small scales. In this case, dissipative mechanisms (as a consequence of the “primary” magnetic reconnection) overcome the turbulent energy during plasma heating.

axion origin – the so-called universal Ballegooijen-Fan-Fisher model (Sec. II A), which are generated by the magnetic buoyancy of practically empty tubes, and as a consequence, their rise from the tachocline to the solar surface (Figs. 2-4). Another goal is the essence of the physics

of the primary and secondary reconnection of magnetic flux tubes in the lower layers of the tachocline (Sect. II B), which is directly related to the observed features of the cycle of both double sunspot maxima (see Sect. II B 2) and the tilt angle of Joy’s law (see Sect. II B 1). Moreover, both effects (see Sect. II A-II B) are caused by the existence (of dark matter?) – solar axions generated in the core of the Sun.

#### A. Radiative $(dQ/dt)_1$ and convective $(dQ/dt)_2$ heatings with the concern of the Parker-Biermann cooling effect and axions of photon origin

The first problem is devoted to the study of the effect of virtually empty magnetic tubes and the phenomenon of solar axions.

The assumption that the virtually empty magnetic tubes (Fig. 2) are neutrally buoyant ( $\rho_{\text{int}} = \rho_{\text{ext}}$  [52]) implies that the temperature inside these tubes is lower than that of the ambient medium (Fig. 2 and Fig. 4a). This leads to the heat inflow, and consequently, the flux tube rises up (see [55] or Sect. 8.8 in [56]). For a horizontal tube with a cross-section of radius  $a$  the rise velocity follows from the Parker’s analysis ([55, 56], also Eq. (60)

## Magnetic reconnection in the lower layers

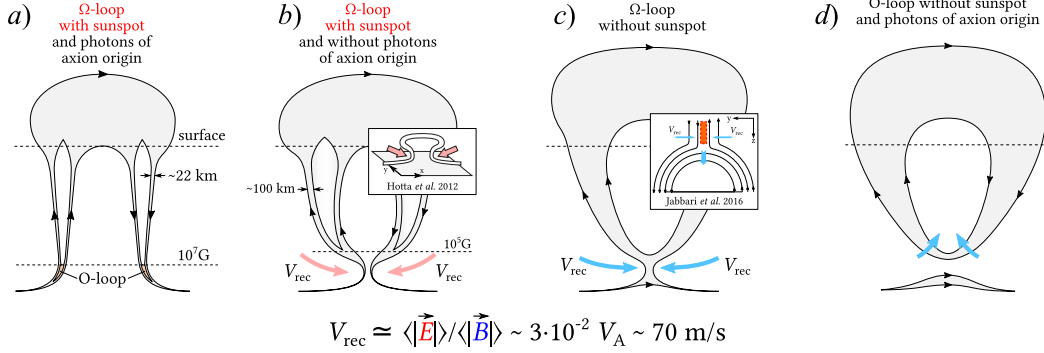


FIG. 4. Sketch of primary or secondary magnetic reconnection near the tachocline. (a) The  $\Omega$ -loop forms a sunspot shadow (with photons of axion origin from O-loops associated with the **primary reconnection**) due to the indirect thermomagnetic EN effect in the tachocline, but **without secondary reconnection**; (b) The  $\Omega$ -loop with a spot in the presence of **secondary reconnection, but without photons of axion origin** (see b,c); the pink arrows show the upward convective flow between the “legs” of the  $\Omega$ -loop as it rises from the tachocline to the visible surface of the Sun; (c) The  $\Omega$ -loop with secondary reconnection and without a sunspot; (d) The O-loop without spots and reconnection. Passing stages (a), (b), (c) (from left to right), the convection around the ascending  $\Omega$ -loop “closes” it at the base (d) and, thus, a free O-loop is formed, and the initial configuration of the azimuthal field is restored near the tachocline. The blue arrows show the motion of matter leading to the connection of the “legs” of the loop and their “flying away” from the surface of the Sun.

in [57]):

$$v_{\text{rise}} = 2 \frac{H_p}{\tau_d} \frac{B^2}{8\pi p_{\text{ext}}} \left( -\delta + 0.12 \frac{B^2}{8\pi p_{\text{ext}}} \right)^{-1}, \quad (3)$$

where  $H_p = \Re T_{\text{ext}}/g = p_{\text{ext}}/g\rho_{\text{ext}} = 0.08R_{\text{Sun}}$  [58–60] is the pressure scale height at the tachocline,  $T_{\text{ext}}$  and  $p_{\text{ext}}$  are the external gas temperature and pressure,  $\delta \equiv Y = \nabla_e - \nabla_{ad} = -c_p^{-1}dS/d\xi = -c_p^{-1}H_p dS/dz$  is the dimensionless entropy gradient (see [57]),  $\nabla_e \equiv d \ln T_e / d \ln p_e$  and  $\nabla_{ad} \equiv (\partial \ln T_e / \partial \ln p_e)_s$  are the local and adiabatic temperature gradients in external and internal plasma [61–63],  $s$  is the specific entropy,  $c_p$  is the heat capacity at constant pressure, and  $\tau_d$  is the rise time of the radiative heating of the magnetic flux tube:

$$\tau_d = \frac{c_p \rho a^2}{k_e} \simeq c_p \rho a^2 \left[ \frac{c_p F_{\text{tot}}}{g} \left( 1 + \frac{2\ell_{ov}}{5H_p} \right)^\nu \right]^{-1}. \quad (4)$$

where for the fully ionized gas  $c_p = 2.5\Re = 2.5p_{\text{ext}}/\rho_{\text{ext}}T_{\text{ext}}$  ( $\Re$  is the equation of state  $p_{\text{ext}} = \rho_{\text{ext}}\Re T_{\text{ext}} = nk_B T_{\text{ext}}$  [58]),  $T(z)$  and  $\rho(z)$  are the mean temperature and density;  $k_e$  is the radiative heat conductivity (see Eq. (35) in [57]);  $\ell_{ov} \approx 0.37H_p$  [62, 63] is the thickness of the overshoot layer; the total radiative energy flux  $F_{\text{tot}} = L/(4\pi r^2)$  depends on the Sun luminosity  $L$ ;  $g$  is the gravitational acceleration.

Next we apply the condition of hydrostatic equilibrium,  $dp/dz = -\rho g$ , when the adiabatic temperature gradient  $(dT/dz)_{ad} = g/c_p$  may be used, and the neutral buoyancy of the flux tube in the overshoot zone  $(|\delta T|/T_{\text{ext}})^{-1} \sim \beta \equiv 8\pi p_{\text{ext}}/B^2$ . This way we are able

to estimate the time of the radiative and/or convective diffusion  $\tau_d$  (see Eq. (4)) of the flux tube:

$$\tau_d = \frac{c_p \rho a^2}{k_e} \approx |\delta T| c_p \rho \frac{a^2}{(1.148)^\nu \delta z |F_{\text{tot}}|}, \quad (5)$$

where

$$\delta z \sim (1.148)^{-\nu} \frac{1}{2} \left( \frac{a}{H_p} \right)^2 H_p \frac{\nabla_e}{\nabla_{\text{rad}}}, \quad \text{where } \nu \geq 3.5, \quad (6)$$

$$F_{\text{tot}} = \frac{L}{4\pi R_{\text{tach}}^2} = H_p \frac{\nabla_{\text{rad}}}{\nabla_e} \left( \frac{dQ}{dt} \right)_1. \quad (7)$$

Here  $\nabla_{\text{rad}} = (\partial \ln T_{\text{ext}} / \partial \ln p_{\text{ext}})_{\text{rad}}$  is the radiative equilibrium temperature gradient;  $(dQ/dt)_1$  is the rate of radiative heating, which only depends on the thermodynamic parameters  $k_e$  and  $T_{\text{ext}}$  of the ambient plasma, depending only on the radial distance from the Sun center [57, 62].

As a result, it is not difficult to show that the van Ballegoijen model combining equations (3)-(7) gives the final expression for the rise time by radiation heating  $(dQ/dt)_1$  from the boundary layer of the overshoot to the solar surface,

$$\tau_d \approx \frac{2}{\beta} T_{\text{ext}} \left[ \frac{1}{c_p \rho_e} \left( \frac{dQ}{dt} \right)_1 \right]^{-1}, \quad (8)$$

at which we have a very important (see section IIB1) value of

$$\tau_d \approx 5 \frac{1}{\beta} p_{ext} / \left( \frac{dQ}{dt} \right)_1 \approx 0.81 \cdot 10^8 \text{ sec} \approx 2 \text{ years}, \quad (9)$$

by means of  $1/\beta = B^2/8\pi\rho_{ext} \approx 2.9 \cdot 10^{-5}$ , which is identical to the magnetic field  $B \approx B_{eq} \sim 2 \cdot 10^5 \text{ G}$  (see  $B^2/8\pi = p_{ext} = nk_B T_{ext} \approx 1.665 \cdot 10^{13} \text{ erg} \cdot \text{cm}^{-3}$  (at  $0.8R_{Sun}$  (see e.g. Fig. 2)) and  $(dQ/dt)_1 \approx 29.7 \text{ erg} \cdot \text{cm}^{-3} \cdot \text{s}^{-1}$  (see Eq. (18) in [64]).

At the same time, the rate of the MFT rise from the tachocline to the solar surface

$$v_{rise} = H_p \nabla_{ad} \frac{1}{p_{ext}} \left( \frac{dQ}{dt} \right)_1 \left( |\delta| + 0.12 \frac{B^2}{8\pi p_{ext}} \right)^{-1}, \quad (10)$$

$$\nabla_{ad} = \nabla_e \simeq 0.4,$$

at which we have a very important (see Sections II A-II B) value of

$$v_{rise} \approx 1.7 \cdot 10^2 \text{ cm/s}, \quad (11)$$

by means of  $H_p \approx 5.6 \cdot 10^4 \text{ km}$  and  $(|\delta| + 0.12 B^2/8\pi p_{ext}) = (3/5) \times B^2/8\pi p_{ext} + 0.12 \times B^2/8\pi p_{ext} \approx 0.72 \times 2.9 \cdot 10^{-5}$  (see Eqs. (58-60) in [57]), are almost identical to the equations (29)-(30) of [64].

At the same time, it is easy to show that these values

$$v_{rise} = \frac{2.77 H_p}{\tau_d}, \quad (12)$$

provide a simple relationship between the rise time and the rate of ascent of the magnetic flux tube from the overshoot boundary layer to the surface of the Sun.

Surprisingly, these equations (Eqs. (8) and (10)) are almost identical to equations (29) and (30) from [64], which arise from completely different equations (60)-(61) of [49].

Unlike the special van Ballegooijen model, we adopt the universal model of MFTs with

$$v_{rise} = 2 \frac{H_p}{\tau_d} \frac{B^2}{8\pi p_{ext}} \left( -\delta + 0.12 \frac{B^2}{8\pi p_{ext}} \right)^{-1}, \quad (13)$$

where

$$\tau_d = \frac{c_p \rho a^2}{k_e} \left\{ \left( \frac{dQ}{dt} \right)_1 \left[ 1 + \left( \frac{dQ}{dt} \right)_2 / \left( \frac{dQ}{dt} \right)_1 \right] \right\}^{-1},$$

Here the second term  $(dQ/dt)_2$  represents a convective diffusion across the flux tube that is due to the temperature difference ( $\delta T \equiv T - T_e$ ) between the flux tube and the external plasma (see [64]).

Using simple calculations of equations (3) and (13) for MFTs, it is easy to show that with the help of the

$$\frac{dQ}{dt} = \left( \frac{dQ}{dt} \right)_1 + \left( \frac{dQ}{dt} \right)_2 \quad (14)$$

of the universal model

$$\tau_d \approx \frac{2}{\beta} T_{ext} \left[ \frac{1}{c_p \rho_e} \frac{dQ}{dt} \right]^{-1}, \quad (15)$$

and

$$v_{rise} = H_p \nabla_{ad} \frac{1}{p_{ext}} \frac{dQ}{dt} \left( -\delta + 0.12 \frac{B^2}{8\pi p_{ext}} \right)^{-1}, \quad (16)$$

$$\nabla_{ad} = \nabla_e \simeq 0.4,$$

is the general case of the so-called universal model of the van Ballegooijen-Fan-Fisher, which is completely identical to equation (27) of the model [64]:

$$\frac{d\Delta\rho}{dt} = \rho_e \frac{v_{rise}}{H_p} \left[ \delta + \left( \frac{1}{\gamma} - \frac{2}{\gamma^2} \right) \frac{1}{\beta} - \frac{1}{\gamma} \frac{\Delta\rho}{\rho_e} \right] + \quad (17)$$

$$\frac{2}{\gamma\beta} \rho_e \left[ \frac{\partial(v \cdot I)}{\partial s} - \vec{v} \cdot \vec{k} \right] + \frac{\rho_e}{p_e} \nabla_{ad} \left[ \left( \frac{dQ}{dt} \right)_1 + \left( \frac{dQ}{dt} \right)_2 \right],$$

where in case of quasi-static rising, it is necessary apply  $(d\Delta\rho/dt)$  and  $\Delta\rho$  to zero (see equation (27) of [64]). Furthermore, according to [64], for simplicity, the lifting of a uniform horizontal magnetic flux tube in the region of a plane-parallel overshoot region is considered, under which the conditions  $\partial(v \cdot I)/\partial s = 0$  and  $\vec{v} \cdot \vec{k} = 0$  can be used in equation (27) of [64]:  $I \equiv \partial r/\partial s$  is the unit vector tangential to the flux tube, and  $k \equiv \partial^2 r/\partial s^2$  is the tube's curvature vector.

It should also be recalled that, taking into account the presence of subadiabaticity  $\delta < 0$  (see Eq. (58) in [57], Eq. (27) in [64], and also Fig. 5) of the overshoot tachocline and using, according to [57], non-local mixing length theory [57, 58, 65–67], it can be shown that thin, neutrally buoyant flow tubes, stable in a stratified medium, provided that its field strength  $B$  is smaller than a critical value  $B_c$  [57], which is approximately given by

$$\frac{B_c^2}{8\pi p_{ext}} = -\gamma\delta = -\frac{5}{3}\delta. \quad (18)$$

Ultimately, we call these Eqs. (13)-(18), in honor of these remarkable “solar” physicists, the universal van Ballegooijen-Fan-Fisher model (vanBFF model).

On the other hand, let us remind that on the basis of the holographic mechanism, generating the toroidal magnetic field in the tachocline, the universal model of flux tubes is predetermined by the existence of strong magnetic fields of the order of  $B_{tachoc} \sim 10^7 \text{ G}$ . Since the physics of the holographic mechanism does not involve a magnetic dynamo, we often refer to it as the universal antidynamo vanBFF model. It is determined by the following total energy rate per unit volume:

$$\frac{dQ}{dt} = \left( \frac{dQ}{dt} \right)_1 + \left( \frac{dQ}{dt} \right)_2 = \left( \frac{dQ}{dt} \right)_1 \left[ 1 + \frac{\alpha_1^2}{\nabla_e} \left( \frac{H_p}{a} \right)^2 \frac{1}{\beta} \right], \quad (19)$$

where

$$\left(\frac{dQ}{dt}\right)_1 = -\nabla \vec{F}_{rad} = F_{tot} \frac{\nabla_e}{\nabla_{rad}} \frac{1}{H_p} = k_e \nabla_e \frac{T_e}{H_p}, \quad (20)$$

$$\left(\frac{dQ}{dt}\right)_2 = -k_e \frac{\alpha_1^2}{a^2} (T - T_e), \quad (21)$$

where we used the MFT heating rate which consists of the radiative heating rate  $(dQ/dt)_1$  and convective heating rate  $(dQ/dt)_2$  (see Eqs. (19)–(21), Eqs. (13) and (19) in [64] and Eqs. (8)–(9) in [67]); the approximate ratio  $|\delta T|/T_{ext} \sim 1/\beta$ ; the parameter  $\alpha_1^2 \approx 5.76$  [64, 67];  $F_{rad}$  is the radiative energy flux (see Eq. (15) in [64], and also Eq. (6) and Fig. 1 in [68]);  $\nabla_e \sim 1.287 \nabla_{rad}$  (see Table 2 in [56]);  $H_p/a$  is the factor for the lower convection zone (see [69]), where it was previously believed that  $a = (\Phi/\pi B_{tacho})^{1/2} \leq 0.1 H_p$  (see 3.2.1 in [57], 5.6.1 in [69]) with an average value of typical magnetic flux of  $\Phi \sim 10^{20} - 10^{22} Mx$  [70–72].

From this, we understand that it is with the strong fields that a sharp increase in convective heating  $(dQ/dt)_2$  is necessary in the tube, which simultaneously leads to a sharp decrease in the outer width of the ring  $a \equiv a_{conv}$  (between the O-loop and the tube walls in Fig. 4a) in a practically empty magnetic flux tube (see Fig. 2 and Fig. 4a). In this case, the area of the “ring” of the magnetic tube is approximately equal to  $2\pi r \times a_{conv}$ , where  $r$  is the radius of the magnetic tube, and  $a_{conv}$  is the width of the “ring”.

What is the physics behind the appearance of the “ring” between the O-loop and the walls of the magnetic tube (see Fig. 5; also Fig. 2)? In simple words, one can say the following. The appearance of the “ring” cross-section is, as a consequence, the result of the production of both axion-origin photons (by converting solar axions into photons in the tachocline) and photon-origin axions (through the conversion of high-energy photons from the radiation zone to axions in the tachocline). From here, on the one hand, the axions of photonic origin are the part of the manifestation of the mean free path of axion origin photons from the tachocline to the photosphere. On the other hand, they are the part of the manifestation of magnetic tube “ring”, where the convective heating  $(dQ/dt)_2$  dominates over the radiation heating  $(dQ/dt)_1$ .

At the same time, we remember that anticorrelated 11-year ADM density modulations in the Sun interior and the ADM around BH (see Sect. 3 in [14]) are not only interconnected, but simultaneously, as consequence, are driving the 11-year modulations of the solar axion density (see Eqs. (27)–(28) in [14]).

As a result, assuming 11-year variations in convective heating  $(dQ/dt)_2$  in the form of a maximum and minimum in the width of the “ring”  $a \equiv a_{conv}$  (between the O-loop and the tube walls in Fig. 5), we apply a new analysis of the universal vanBFF model (see Eqs. (19)–(21) similar to the last part of Eqs. (13) and (19) in [64]), where the values such as the magnetic flux  $\Phi$  (see [71, 72])

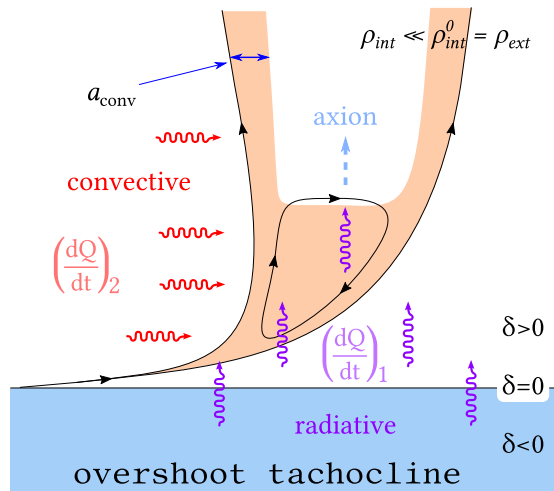


FIG. 5. A sketch of the magnetic tube born anchored to the tachocline and risen to the solar surface by the neutral buoyancy ( $\rho_{ext} = \rho_{int}^0$ ). The strong convection suppression inside the tube leads to the abrupt decrease of temperature and density ( $\rho_{int}^0 \gg \rho_{int}$ ), which in its turn leads to the significant decrease in gas pressure above the umbra (sunspot). At the top of the overshoot tachocline the first term  $(dQ/dt)_1$  characterizes the radiative heating which depends on the thermodynamic quantities  $k_{ext}$  and  $T_{ext}$  of the external plasma, changing with the distance from the center of the Sun only (see Eq. (20)). The second term  $(dQ/dt)_2$  represents the diffuse radiation through the flux tube because of the temperature difference between the tube ring (see  $a \equiv a_{conv}$  between the O-loop and the tube walls) and the surrounding plasma (see Eq. (21)). The keV photons (see Fig. 2 in [73]) coming from the radiation zone are turned into axions in the horizontal magnetic field of the O-loop (see Fig. 2). Therefore, the radiative heating almost vanishes in the virtually empty magnetic tube. The base of the convection zone is defined as a radius at which the stratification switches from almost adiabatic ( $\delta = \nabla_e - \nabla_{ad} = 0$ ) to sub-adiabatic ( $\delta = \nabla_e - \nabla_{ad} < 0$ ). Meanwhile, the external plasma turns from sub-adiabatic to super-adiabatic ( $\delta = \nabla_e - \nabla_{ad} > 0$ ).

and the magnetic fields at the tachocline ( $3.6 \cdot 10^7 G$  in Fig. 2) are consistent with known observational data:

- values of the magnetic tube (see Fig. 4a), based on the physics of convective heating  $(dQ/dt)_2$ , are related to the radius of the “ring” between the O-shaped loop and the walls of the magnetic tube (Fig. 5), and correspond exactly to the “observed” values of the ratio between the maximum and minimum magnetic flux and the magnetic field at the tachocline [69, 71, 72]. Therefore, we are interested in the observed magnetic fluxes

$$\Phi_{max} = 2\pi r (a_{conv})_{min} (B_{tacho})_{max} \approx 10^{22} Mx, \quad (22)$$

where  $\Phi_{max} \approx 10^{22} Mx$  is at the maximum of the “measured” magnetic fluxes [71, 72] and the maximum of the “measured” magnetic field MFT  $(B_{tacho})_{max} \sim 3.7 \cdot 10^7 G$  (see Fig. 2), which is associated with the

so-called Etingshausen-Nernst thermomagnetic effect, caused by the Parker-Biermann cooling effect.

Then a minimum of magnetic flux appears

$$\Phi_{min} = 2\pi r (a_{conv})_{max} (B_{tach})_{min} \approx 5 \cdot 10^{21} \text{ Mx}, \quad (23)$$

where  $\Phi_{min} \approx 5 \cdot 10^{21} \text{ Mx}$  is at the minimum of the “measured” magnetic fluxes [71, 72] and the minimum of the “measured” magnetic field MFT  $(B_{tach})_{min} \sim 3.7 \cdot 10^6 \text{ G}$ .

It is very important here that, on the one hand, the anchored magnetic field in the tachocline rises from the bottom of the convective zone to the solar photosphere in the form of thin isolated filaments known as flux tubes (see e.g. [56]), and on the other hand, the well-known nonlinear dynamics of a thin magnetic tube was modeled in the form that has been used by [59]. In this case, the magnetic tube is assumed to be thin in the sense that its cross-sectional radius  $a_{conv}$  is negligibly small with respect to both the atmospheric scale height (i.e.  $a_{conv} \ll H_p$  (see Fig. 5)) and any variation scales along the tube. This means that each magnetic field line is roughly parallel to the axis of the tube, and the Spruit’s model is applicable only to untwisted magnetic tubes.

This raises a rather complicated but simple question: In what way, without twisting, can a real magnetic tube, which is not integral and will not behave as a single object for a very long time [56, 59], be obtained without destruction by hydrodynamic forces?

The answer, oddly enough, is very simple! For an untwisted thin magnetic tube, the pressure balance is always maintained not only along the entire radius of the “ring” between the O-shaped contour and the walls of the magnetic tube (Fig. 5), which is solved without destruction by hydrodynamic forces, but at the same time leads to the suppression of convection along the inner radius of the O-shaped contour due to a sharp decrease in temperature and density (see  $\rho_{int}^0 \gg \rho_{int}$  in Fig. 5). The latter means that in very strong magnetic fields (e.g.  $5 \cdot 10^5 \text{ G} < B < 10^7 \text{ G}$ ) an untwisted thin magnetic tube will, surprisingly, always be perpendicular to the azimuthal direction from the tachocline to the surface of the photosphere!

The physics of this process is briefly as follows. The high-energy photons from the radiation zone through axion-photon oscillations in the O-loop inside the magnetic tube near the tachocline create the so-called axions of photon origin under the sunspot. This means that at such strong magnetic fields, the Parker-Biermann effect of cooling inside the magnetic tube, where the Sun’s gravitational field pulls gas out of the inner tube (as described by hydrostatic pressure, known as the barometric law  $dp/dz = -\rho g$ ), develops due to the “disappearance” of the convective heat transfer  $(dQ/dt)_2$  and, as a consequence, the temperature in the lower part of the magnetic tube with the help of axions of photon origin from photon-axion oscillations in the O-loop near the tachocline. As a result, it opens a free path (in the radial direction!) for photons of axion origin (Rosseland

length; see Fig. B.3 in [14]) from the tachocline to the photosphere (see Fig. 4a)!

From here, using Eq. (22) and Eq. (23), we obtain the cross-section values  $a_{conv}$  (between the O-loop and the tube walls in Fig. 4a) at the minimum

$$(a_{conv})_{min} \sim 22 \text{ km} \approx 3.7 \cdot 10^{-4} H_p \quad (24)$$

and at the maximum

$$(a_{conv})_{max} \sim 220 \text{ km} \approx 3.7 \cdot 10^{-3} H_p, \quad (25)$$

at which the rise time of convective heating of the flux tube from the tachocline to the photosphere (see Eq. (15)) corresponds to the equations

$$(\tau_d)_{conv} = \frac{2}{\beta} T_{ext} \left\{ \frac{1}{c_p \rho_{ext}} \left( \frac{dQ}{dt} \right)_1 \left[ 1 + \frac{\alpha_1^2}{\nabla_e \beta} \left( \frac{H_p}{a_{conv}} \right)^2 \right] \right\}^{-1} \quad (26)$$

$$= \frac{2}{\beta} T_{ext} 2.5 \Re \rho_{ext} \left\{ \left( \frac{dQ}{dt} \right)_1 \left[ 1 + \frac{\alpha_1^2}{\nabla_e \beta} \left( \frac{H_p}{a_{conv}} \right)^2 \right] \right\}^{-1}$$

$$= \frac{5}{\beta} T_{ext} (p_{ext}/\rho_{ext} T_{ext}) \rho_{ext} \left\{ \left( \frac{dQ}{dt} \right)_1 \left[ 1 + \frac{\alpha_1^2}{\nabla_e \beta} \left( \frac{H_p}{a_{conv}} \right)^2 \right] \right\}^{-1}$$

$$= \frac{5}{\beta} p_{ext} \left\{ \left( \frac{dQ}{dt} \right)_1 \left[ 1 + \frac{\alpha_1^2}{\nabla_e \beta} \left( \frac{H_p}{a_{conv}} \right)^2 \right] \right\}^{-1} \quad (27)$$

$$= \frac{5}{\beta} n k_B T_{ext} \left\{ \left( \frac{dQ}{dt} \right)_1 \left[ 1 + \frac{\alpha_1^2}{\nabla_e \beta} \left( \frac{H_p}{a_{conv}} \right)^2 \right] \right\}^{-1} \quad (28)$$

$$\cong \frac{5}{\beta} \rho_{ext} \mu^{-1} m_p^{-1} k_B T_{ext} \left\{ \left( \frac{dQ}{dt} \right)_1 \left[ 1 + \frac{\alpha_1^2}{\nabla_e \beta} \left( \frac{H_p}{a_{conv}} \right)^2 \right] \right\}^{-1} \quad (29)$$

where at the maximum the values of  $(a_{conv})_{min} \approx 3.7 \cdot 10^{-4} H_p$  and  $1/\beta = B^2/8\pi p_{ext} \approx 1$  we represent 11-year variations of the magnetic flux tube in the photosphere for sunspots (see (28) or (27), in the form

$$(\tau_d)_{conv}^{max} \approx 5 \times (6.5 \cdot 10^{13} \text{ erg} \cdot \text{cm}^{-3}) / 3 \cdot 10^9 \text{ erg} \cdot \text{cm}^{-3} \cdot \text{s}^{-1}$$

$$\approx 10^{15} \text{ erg} \cdot \text{cm}^{-3} / 3 \cdot 10^9 \text{ erg} \cdot \text{cm}^{-3} \cdot \text{s}^{-1} \approx 1.1 \cdot 10^5 \text{ s}, \quad (30)$$

or

$$(\tau_d)_{conv}^{max} \approx 1.1 \cdot 10^5 \text{ s} \sim 1.3 \text{ day}, \quad (31)$$

where  $p_{ext} = 6.53 \cdot 10^{13} \text{ erg/cm}^3$  (see [49]),  $T_{ext} = 2.3 \cdot 10^6 \text{ K}$  and  $\rho_{ext} = 0.2 \text{ g/cm}^3$  [49];  $c_p = 2.5 \Re = 2.5 p_{ext} / \rho_{ext} T_{ext}$  ( $\Re$  is the gas constant in the equation of state  $p_{ext} = \rho_{ext} \Re T_{ext} = n k_B T_{ext}$  [58]);  $\mu = 0.58$  is mean molecular weight of hydrogen in overshoot tachocline,

$m_p \cong 1.67 \cdot 10^{-24} \text{ g}$  is the proton mass: "2018 CODATA Value: proton mass", The NIST Reference on Constants, Units, and Uncertainty, 20 May 2019;  $k_B = 1.38 \cdot 10^{-23} \text{ J/K}$ ;  $(dQ/dt)_1 \approx 29.7 \text{ erg} \cdot \text{cm}^{-3} \cdot \text{s}^{-1}$  (see Eq. (18) in [64]) is the rate of radiative heating;  $\alpha_1^2 \approx 5.76$  [64, 67];  $\nabla_e \approx 0.4$  (see Table 2 in [61]);  $H_p = \Re T_{ext}/g = p_{ext}/g\rho_{ext} = 0.08R_{Sun}$  [58–60];  $a_{conv}^{min} \sim 3.7 \cdot 10^{-4}H_p$  (see Eq. (24)).

And, as a consequence, the magnitude of the MFT rise speed (see Eq. (16)) will be equal to

$$(v_{rise})_{conv} = \frac{2.77H_p}{(\tau_d)_{conv}}, \quad (32)$$

both at the maximum of the solar cycle

$$(v_{rise})_{conv}^{max} \sim 1.40 \text{ km/s}, \quad (33)$$

which are almost identical to the observational data of the known works (see about 1.4 km/s in [74–77]), and at the minimum of the solar cycle

$$(v_{rise})_{conv}^{min} \sim 0.14 \text{ km/s}, \quad (34)$$

which are almost identical to the observational data of the known works (see about  $\sim 0.15 \text{ km/s}$  in [78]), from which we obtain the “minimum” time of increase of convective heating  $(dQ/dt)_2$  of the flux tube from the tachocline to the photosphere (see Eq. (15)), which corresponds to the equation

$$(\tau_d)_{conv}^{min} \approx 10^6 \text{ s} \sim 10 \text{ days}, \quad (35)$$

where  $p_{ext} = (nk_B T)_{min} = 3.56 \cdot 10^{13} \text{ erg/cm}^3$ ,  $T_{ext} = 10^6 \text{ K}$ ,  $\rho_{ext} \approx 0.25 \text{ g/cm}^3$  (see Eq. (27)).

Ultimately, these Eq. (32) are the source of the first (fast in time) maximum of solar activity (e.g. sunspots) from the observed double maxima of 11-year cycles, while the second (two-year in time) maximum of sunspots is associated with observational data on the slope of Joy’s law (see Fig. 8b<sub>2,c</sub> on the right).

This raises an intriguing point regarding helioseismology. One of the first solutions in our section is the buoyancy of a virtually empty magnetic flux tube in strong magnetic fields of  $\sim 10^7 \text{ G}$  near the tachocline, determined by the thermomagnetic Ettingshausen-Nernst effect (see Appendix A in [14]), manifesting itself as “visible” sunspots on the solar surface. This is due to the fact that helioseismological inversions, which are well suited not only for studying the rotation and structure of the Sun, can sometimes be well suited due to the mediated effects of very strong magnetic fields at empty magnetic flux tubes. Let us repeat once again that it is the existence of empty magnetic flux tubes that allows photons of axion origin to “rush” past the tachocline to the photosphere both at high speed (see  $\sim 1.4 \text{ km/s}$  in [74–77]) and at short times (see  $\sim 1.3 \text{ days}$  for Eqs. (31)–(32))! Thus, they can unequivocally confirm the presence of a magnetic field in the solar tachocline exceeding  $> 10^5 \text{ G}$  to, for example,  $10^7 \text{ G}$ . On the other hand, it is the

existence of “visible” sunspots in such strong fields that causes the dynamo effect to completely disappear.

The answer, surprisingly, is quite simple. It means that the “measured” velocity (maximum about  $\sim 1.4 \text{ km/s}$  [74–77] and minimum about  $\sim 0.15 \text{ km/s}$  in [78]) of magnetic flux tubes, which are associated with structural changes, for example, in the form of cross-sections of these tubes at the maximum ( $\sim 10^{22} \text{ Mx}$ ) or minimum ( $5 \cdot 10^{21} \text{ Mx}$ ) of the “measured” magnetic fluxes [71, 72], can be easily determined at the maximum  $\sim 10^7 \text{ G}$  or minimum  $\sim 10^6 \text{ G}$  values of the magnetic fields (see Eqs. (22)–(23)). The modernity of this considered helio-seismological inversion remains to this day!

In other words, the modernity of this well-thought-out helioseismological inversion remains to this day!

## B. Physics of primary and secondary reconnection of magnetic flux tubes in the lower layers of the tachocline

The problem is devoted to the physics of primary and secondary magnetic reconnection in the lower layers of the tube, which is directly related to the observed features of the cycle of both double maxima of sunspots and the tilt angle of Joy’s law.

First, let us recall the essence of the primary reconnection inside magnetic tubes near the tachocline ( $B \sim 10^7 \text{ G}$ ), which generates the O-loop (see Fig. 4d), and thus participates in the formation of axion origin photons (see Fig. 2, left) and axions of photon origin (see Fig. 2, right) from the O-loop to the photosphere, is the source of sunspots, which (due to the cooling of the Parker-Biermann effect inside the tube) rise from the tachocline to the surface of the Sun.

On the other hand, we are interested in the essence of the very important secondary magnetic reconnection (see Fig. 6b), which is the source of the observed double maxima of one sunspot cycle – it shifts by 2.5 years between the primary and secondary solar maxima when the magnetic tube rises, and is associated with both the observational data on the tilt angle of Joy’s law and the “disappearance” of sunspots on the solar surface.

In Fig. 6 one can see the conditions for the secondary reconnection between the O-loop (green lines) and the unipolar part of the  $\Omega$ -loop (blue lines) that can organize them in the lower layer (Fig. 6, left) or in the upper layer (Fig. 6, right), thereby showing the appearance of bipolar magnetic tubes in various versions (Fig. 6c,d and g,h).

From here, since the sunspot cycle is identical to the maxima and minima of the magnetic tube number on the surface of the Sun, we are interested in the physics of the maxima and minima both during the primary reconnection for the time  $(\tau_d)_{conv}$  of the rise of the almost empty magnetic tube from the tachocline to the solar photosphere (see about  $\sim 1 - 2 \text{ days}$  at max in Eq. (31) and about  $\sim 10 \text{ days}$  at min in Eq. 35), and during the secondary reconnection  $(\tau_n)_{rec}$ , which are associated with

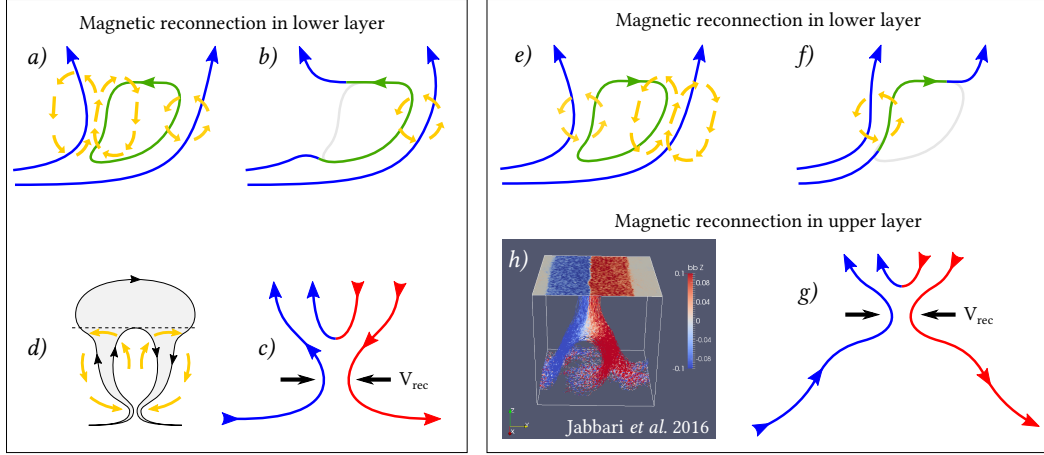


FIG. 6. Topological effects of secondary magnetic reconnection in the lower (left) or upper (right) layers of the magnetic tube. Here, the unipolar part of the  $\Omega$ -loop is rearranged at its base, compressing the  $\Omega$ -loop (blue lines) and, as a consequence, organizing a free O-loop (green lines) (a,e) to form (blue-yellow lines) the first part of the secondary magnetic reconnection (b,f). The yellow lines show the movement of matter leading to the loop connection “leg” (see analogous Fig. 4 in [52]). If the O-loop (primary magnetic reconnection, green lines) can randomly have different directions of magnetic fields, then the secondary magnetic reconnection can generate loop “legs” in different layers, for example, in lower layers (c and d as an analog of Fig. 4b) and upper layers (e and f as an analog of Fig. 4 in [79]).

the features of the tilt angle of Joy’s law (see Fig. 8c), during the rise of the almost empty magnetic tube from the surface of the Sun (see about  $\sim 2$  years in Fig. 8b<sub>2</sub> and c) and, as a consequence, their “disappearance” on the Sun (see about  $< 0.5$  years in Fig. 8c).

1. *Secondary reconnection of the MFT without axions, but with concern of turbulent diffusion and the tilt angle of the Joy law*

The first part of the scenario consists in discussing the physics of magnetic flux tube buoyancy at strong fields and with the participation of axion origin photons (see Fig. 1), associating with the formation of an O-loop (see the existence of primary magnetic reconnection in Fig. 2) inside the magnetic flux tube near the tachocline.

For the condition of neutral buoyancy ( $\rho_{int} = \rho_{ext} \approx 0.2 \text{ g/cm}^3$  [49]; see A.16 in [14], Figs. 2 and 5) and the strong toroidal field of the magnetic tube,  $B_{Sun} = 4.1 \cdot 10^7 \text{ G}$ , as well as the condition of the average width of the “thin” ring  $a_{conv}^{min} \sim 3.7 \cdot 10^{-4} H_p$  (see Eq. (24)) between the O-shaped loop and the walls of the magnetic tube (see Fig. 5), it is easy to recall the estimate of the time  $(\tau_d)_{conv}^{max} \sim 1.3 \text{ days}$  (see Eq. (31)) and velocity  $(v_{rise})_{conv}^{max} \sim 1.40 \text{ km/s}$  (see Eq. (33)), as well as the time  $(\tau_d)_{conv}^{min} \sim 10 \text{ days}$  (see Eq. (35)) and velocity  $(v_{rise})_{conv}^{min} \sim 0.14 \text{ km/s}$  (see Eq. (34)) of the convective rise from the tachocline to the photosphere, which for such large magnetic fields has a significant amount of rise of the magnetic tubes at all latitudes (see Fig. 4a and the red arrows of the magnetic flux tubes in Fig. 7a).

This solution clearly depends on the rise time of the

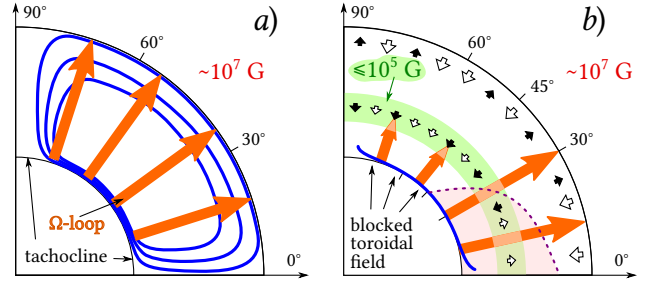


FIG. 7. Scheme of turbulent reconstruction of the toroidal magnetic field in the convective zone (CZ): (a) meridional circulation (closed blue poloidal field lines), which is the source of the toroidal field in the tachocline (thin black lines), and the magnetic buoyancy of the flux tubes (red arrows) with a magnetic field of  $\sim 10^7 \text{ G}$ ; (b) In the CZ, through secondary turbulent reconnection of the magnetic tube near the tachocline (see Fig. 8b<sub>2</sub>,c), effects of both macroscopic turbulent plasma diamagnetism are observed, facilitating the formation of two layers on the surface (see analogous [80–82]) with different vertical directions of horizontal field transfer (see “black” arrows), and the conditions of magnetic field transfer along  $\nabla\rho$  due to small-scale magnetic pulsations, acting against buoyancy. However, in the deep layers in the near-equatorial region, the  $\nabla\rho$  effect provides upward advection, which, on the contrary, directs magnetic buoyancy, and thus, can facilitate the penetration of strong fields to the surface.

magnetic tubes rising from the tachocline to the solar surface. Therefore, the primary magnetic reconnection itself in the lower layers of the magnetic tubes (see Fig. 4a),

is not the final stage of the modeling. The essence of a practically empty tube in strong fields of  $\sim 10^7 G$  is related (through the primary magnetic reconnection) to the physics of the secondary turbulent reconnection of magnetic bipolar structures (see Fig. 4b, and also Fig. 4 in [60]). Here, on its basis, the bipolar part of the  $\Omega$ -loop is reconstructed, compressing the  $\Omega$ -loop (blue lines: see Fig. 4b,c) near the tachocline and simultaneously lifting them (from 2 to 3 years) to the surface of the Sun, and, as a consequence, after some time (from several days to several months (see [83, 84]) a free O-loop appears (blue lines in Fig. 4d), which eventually “disintegrates” or, more precisely, the O-loop (without spots) flies away from the surface of the Sun (see Fig. 4d).

This raises a rather unexpected but important question: How is the secondary magnetic reconnection of flux tubes with  $B_{tach}^{Sun} = B_z = 4.1 \cdot 10^7 G$ , leading to a real sharp decrease in the magnetic field to  $B_{eq} \leq 2 \cdot 10^5 G$  at  $\sim 0.80 R_{Sun}$  (see e.g. Fig. 8b,c), related to the existence of downward turbulent diamagnetic pumping and rotational  $\nabla\rho$ -pumping at relatively low magnetic fields, and as a consequence, at low escape velocities of flux tubes from the solar surface?

In this regard, we obtain an answer to this important question. For this purpose, we consider the second part of the scenario, based on the remarkable idea of L.L. Kitchatinov [84], which includes the generation of the magnetic field of  $\leq 2 \cdot 10^5 G$  near the bottom of the convective zone and transfer of the toroidal field from the deep layers at different latitudes. It is very important that the efficiency of the magnetic buoyancy transfer is associated with the participation of two processes: macroscopic turbulent diamagnetism [85–87] and rotational  $\nabla\rho$ -pumping [84].

Let us note some important properties of macroscopic turbulent diamagnetism. It is known that Zel’dovich [85, 86] and Spitzer [87] in 1957 discovered the diamagnetism of inhomogeneously turbulent conducting liquids, in which the inhomogeneous magnetic field moves as a single whole. In this case the turbulent fluid, for example, with nonuniform effective diffusivity  $\eta_T \approx (1/3)vl$  (see Fig. 1 in [88], and also [85–87]) behaves like a diamagnetic one and carries the magnetic field with the effective velocity [89]

$$\vec{v}_{dia} = -\frac{1}{2}\nabla\eta_T, \quad (36)$$

where  $l$  is the mixing length of turbulent pulsations, and  $v = \sqrt{\langle v^2 \rangle}$  is the root-mean-square velocity of turbulent motion. The minus sign on the right in Eq. (36) shows the meaning of turbulent magnetism: it is not paramagnetic magnetism, so magnetic fields repel from regions with relatively high turbulent intensity. In other words, macroscopic turbulent plasma diamagnetism and, as a consequence, the so-called macroscopic diamagnetic effect (see [90, 91]) in the physical sense is the displacement of the averaged magnetic field  $B$  from regions with increased intensity of turbulent pulsations to regions with

less developed turbulence [92, 93].

However, there is an interesting problem of the diamagnetic process caused by inhomogeneous turbulent intensity with allowance for the total nonlinearities in the magnetic field. This is due to the fact that up to the present time analytical estimates have been obtained only for the limiting cases of weak and strong magnetic fields. For example, at strong magnetic fields of flux tubes, at  $B > 10^5 G$ , e.g.  $\geq 10^7 G$ , the diamagnetic effect becomes almost negligible, in particular, strong magnetic damping of diamagnetism  $\sim B^{-3}$  is obtained for super-equipartitions of fields [94] when turbulence is close to two-dimensional [85]. On the other hand, for very weak fields the diamagnetic pumping, which is predetermined by the intensity of turbulence at  $B < 10^5 G$ , is a very effective process [94].

Among the known limiting cases of weak and strong magnetic fields from the tachocline to the surface, we are interested, in the addition to the portions of strong fields (via the secondary Lazaryan-Vishniac reconnection (see [95–97], and also §III and §IX in [98]) near the tachocline, which have a very slow Sweet-Parker velocity  $(V_{rec})_2$  (see [99, 100]) for Fig. 8b<sub>2</sub>), the part of the weak magnetic field from  $0.8 R_{Sun}$  to near  $0.85 R_{Sun}$  (see Fig. 8b<sub>2</sub>,c), which constitutes the super-equipartitions of field  $B \geq B_{eq}$  and is the source of two processes: diamagnetic pumping, and rotational  $\nabla\rho$ -pumping. This is due to the fact that the secondary magnetic reconnection of the flux tubes (see Figs. 6b,d,f,g) leads to the real increase in the upward magnetic field to  $B \approx 2 \cdot 10^5 G$  at  $\sim 0.8 R_{Sun}$ , which is identical to the  $1/\beta = B^2/8\pi p_{ext} \approx 2.9 \cdot 10^{-5}$  (see e.g. Eq. (9), and Fig. 8b<sub>2</sub>,c). This means that the real toroidal magnetic flux tube is a consequence of the formation of the secondary reconnection, which generates both the “anti-buoyant” effects of downward turbulent diamagnetic transport and the rotational effect of the magnetic  $\nabla\rho$ -pumping at polar latitudes, and the “buoyant” effects of magnetic flux tubes at equatorial latitudes as a result of the upward rotational effect of magnetic  $\nabla\rho$ -pumping.

In this regard, we consider turbulence with quasi-isotropic spectral tensor [84, 102], which is certainly the simplest representation for inhomogeneous turbulence (see Eq. (2.12) in [93]). As a consequence, the information on the spectral properties of turbulence (given by Eqs. (2.12)-(2.16) from [93]) is sufficient to reduce the expression for the average electromotive force  $\varepsilon$  (see Eq. (2.1) [93]) to its traditional form, where only integrations over the wave number  $k$  and frequency  $\omega$  remain. After such shortening it is possible to get (see Eq. 3.1 in [93])

$$\vec{F} = (\vec{v}_{dia} + \vec{v}_{dens}) \times \vec{B} \quad (37)$$

with the speed of turbulent diamagnetic transfer

$$\vec{v}_{dia} = -\nabla \int_0^\infty \Re_{dia}(k, \omega, B) \frac{\eta k^2 q(k, \omega, x)}{\omega^2 + \eta^2 k^4} dk d\omega, \quad (38)$$

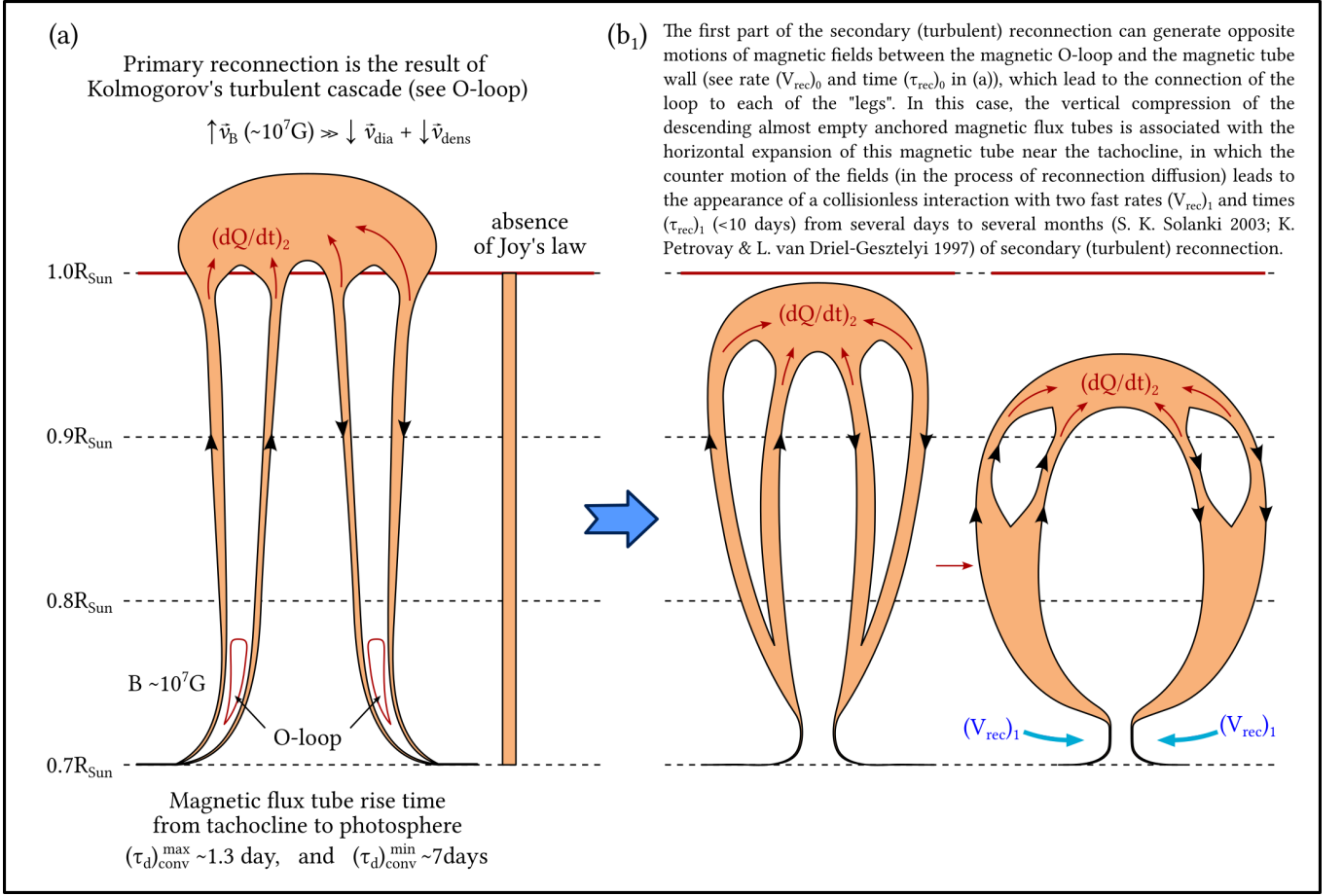


FIG. 8. An alternative theory of magnetic flux tubes in strong fields by means of axion origin photons associated with primary and secondary reconnections. [Ref: S.K. Solanki (2003) [101], K. Petrovay & L. van Driel-Gesztelyi (1997) [83].]

where  $q$  stands for the local velocity spectrum, and the rate of rotational magnetic advection caused by the vertical heterogeneity of the fluid density in the convective zone, i.e. the magnetic  $\nabla\rho$ -pumping effect,

$$\vec{v}_{dens} = \frac{\nabla\rho}{\rho} \int_0^\infty \Re_{dens}(k, \omega, B) \frac{\eta k^2 q(k, \omega, x)}{\omega^2 + \eta^2 k^4} dk d\omega. \quad (39)$$

The effective speeds  $v_{dens}$  and  $v_{dia}$  are consequences of the non-uniformity of density and of turbulence intensity, respectively, where the latter is attributed to the known diamagnetic pumping. The velocities (39) and (38) depend on the magnetic field through the kernels  $\Re_{dens}$  and  $\Re_{dia}$ .

We are interested in the problem of reconstructing a strong toroidal field of flux tubes  $\sim 10^7 G$  (see Figs. 7a,b for the magnetic tube profile, and Figs. 8a,b,c for the magnetic tube in full face), transform the regions of the average magnetic field  $B \sim 2 \cdot 10^5 G$  in the convective zone (see Figs. 8b,c), and thereby allow the organization of the amazing balance between the magnetic buoyancy,

turbulent diamagnetism, and the rotationally modified  $\nabla\rho$ -effect.

In this regard, we first consider the physics of linear magnetic diffusivity, which is known to govern two processes: macroscopic turbulent diamagnetism and rotational  $\nabla\rho$ -pumping. This is because the standard theory of the turbulent mixing length  $l$  and the characteristic velocity of the dominant eddies  $u$  yields a diffusion coefficient  $\eta_T = (1/3)ul$ , that depends directly on the diamagnetic pumping rate  $v_{dia} = -\nabla\eta_T/2$  and, indirectly, on the rotational  $\nabla\rho$ -pumping  $v_{dens}$ .

Here we assumed that, according to Figs. 8b<sub>2</sub>,c, the radial profile of turbulent diffusion is a smooth-convex function with a maximum,  $\eta_T \approx 10^{11} \text{ cm}^2/\text{s}$ , approximately in the middle of the CZ at a depth of  $z = 1.30 \cdot 10^5 \text{ km}$  at  $\sim 0.8R_{Sun}$ , which is described by the distance of  $2.3 \cdot 10^4 \text{ km}$  between  $0.8R_{Sun}$  and near  $0.85R_{Sun}$  (see Figs. 8b<sub>2</sub>,c) and with the depth of the bottom of the convective zone  $z_0 \approx 1.84 \cdot 10^5 \text{ km}$  (see [103–105]).

In order to consider the balance of the three velocities  $v_B$ ,  $v_{dia}$ , and  $v_{dens}$ , it is necessary to apply the widely used approximation of the mixing length (see

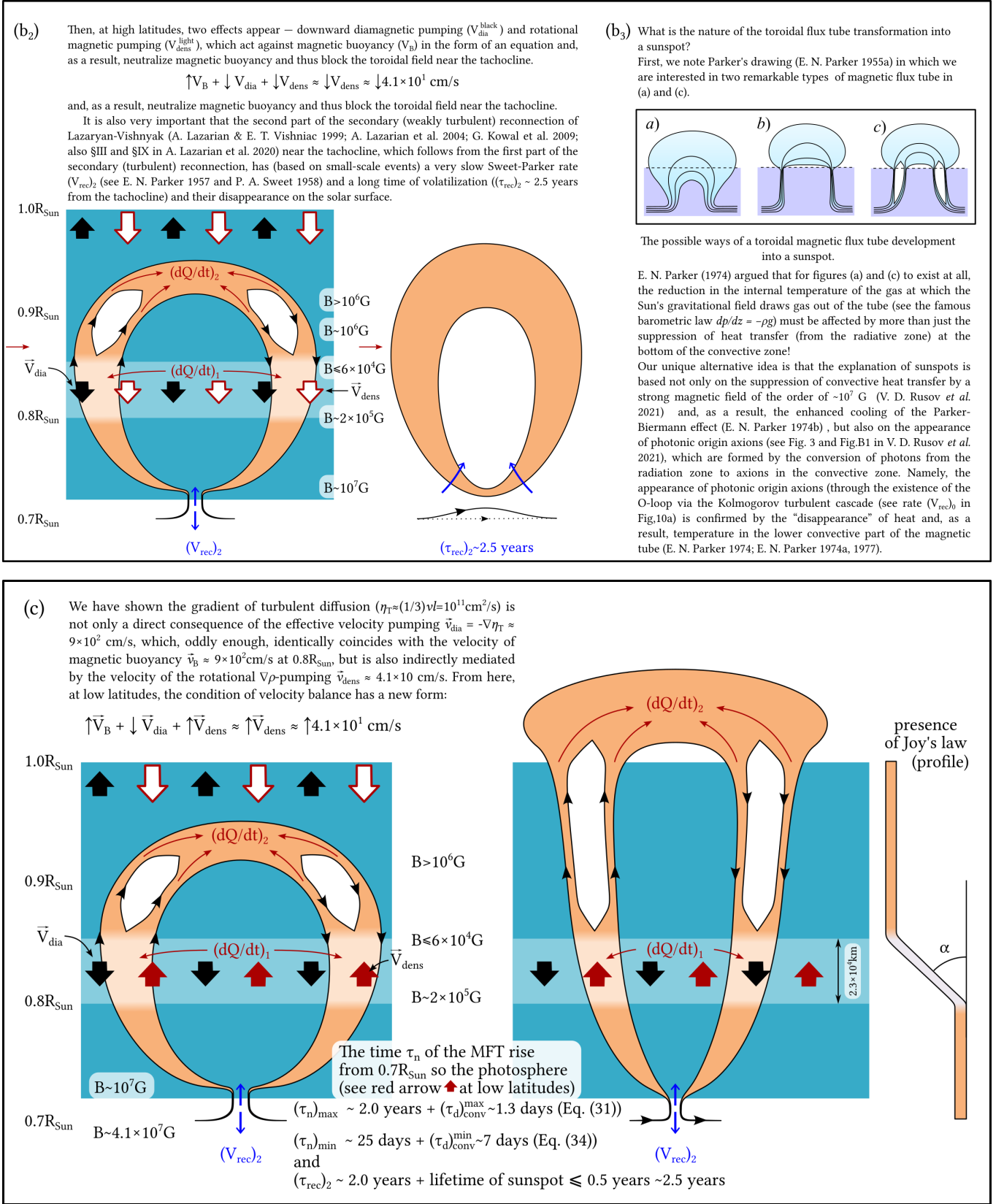


FIG. 8. (cont.) An alternative theory of magnetic flux tubes in strong fields by means of axion origin photons associated with primary and secondary reconnections. [Ref: A. Lazarian & E. T. Vishniac (1999) [95]; A. Lazarian et al. (2004) [96], (2020) [98]; G. Kowal et al. (2009) [97]; P. A. Sweet (1958) [100]; E. N. Parker (1955a) [6], (1957) [99], (1974) [11], (1974a) [12], (1974b) [10], (1977) [13]; V. D. Rusov et al. (2021) [14]]

e.g. [58, 106–108]), which, according to [84], fully satisfies this goal. This approximation will be understood as the replacement of nonlinear terms along with time derivatives in the equations for fluctuating fields by means of  $\tau$ -relaxation terms, i.e. instead of equations (3.1) and (3.9) from [84], we now have the equation of the radial speed of the toroidal field in the convection zone

$$v_{dens}^{light} = \tau \langle u^2 \rangle^\circ \frac{\nabla \rho}{\rho} \left[ \phi_2(\hat{\Omega}) - \cos^2 \theta \cdot \phi_1(\hat{\Omega}) \right] \approx \quad (40)$$

$$\approx 6v_p \left[ \phi_2(\hat{\Omega}) - \cos^2 \theta \cdot \phi_1(\hat{\Omega}) \right] = \quad (41)$$

$$= -\frac{3\kappa g}{(\gamma-1)c_p T} \left[ \phi_2(\hat{\Omega}) - \cos^2 \theta \cdot \phi_1(\hat{\Omega}) \right], \quad (42)$$

and **firstly**, it can be shown that at  $\eta_T \approx 10^{11}$  cm/s, we have

$$v_{dens}^{light} \sim 3 \times \eta_T \times g_{0.8R_{Sun}} / (\gamma-1)c_p T_{0.8R_{Sun}} \approx 4.1 \cdot 10^1 \text{ cm/s}, \quad (43)$$

where  $\tau \approx l / (\langle u^2 \rangle^\circ)^{1/2}$  is a typical lifetime of a convective eddy;  $l$  is the mixing length;  $\langle u^2 \rangle^\circ$  is the mean intensity of fluctuating velocities for original turbulence;  $\theta$  is the latitude (scalar);  $e_r \nabla \rho / \rho = -e_r g / [(\gamma-1)c_p T]$ , where  $e_r$  is the radial unit vector;  $T \cong 1.352 \cdot 10^6$  K is the temperature at  $0.8R_{Sun}$  [49];  $g = g_0(R_{Sun}/r)$  is the gravity, where  $g_0 = 2.74 \cdot 10^4$  cm/s<sup>2</sup> is the surface value of solar gravity, and  $g_{0.8R_{Sun}} = 4.22 \cdot 10^4$  cm/s<sup>2</sup> at  $0.8R_{Sun}$ ;  $c_p = 3.4 \cdot 10^8$  cm<sup>2</sup>s<sup>-2</sup>K<sup>-1</sup> (fully ionized hydrogen) is the specific heat at constant pressure;  $\gamma = 5/3$  is the ratio of specific heats  $c_p/c_V$ ;  $3\kappa = \tau \langle u^2 \rangle^\circ$ , where  $\kappa \equiv \eta_T \approx 10^{11}$  cm<sup>2</sup>/s is turbulent diffusivity coefficient, and the mixing length relation  $\langle u^2 \rangle^\circ = -\nabla \Delta T l^2 g / (4T)$ , where the  $\nabla \Delta T$  is superadiabatic temperature gradient;  $v_p = (1/6)\tau \langle u^2 \rangle^\circ (\nabla \rho / \rho)$  is the velocity of the magnetic field transfer caused by the density gradient (see Eq. (36) in [109]);  $\hat{\Omega} = Co = 2\tau\Omega$  is the Coriolis number (reciprocal of the Rossby number), where  $\Omega$  is the rotation speed,  $\tau$  is the turnover time, and the functions

$$\phi_n(\hat{\Omega}) = (1/8)I_n(\Omega, k, \omega) \quad (44)$$

(see  $I_1$  and  $I_2$  in Eqs. (3.12) and (3.21) in [84]) are

$$\phi_1(\hat{\Omega}) = \frac{1}{4\hat{\Omega}^2} \left[ -3 + \frac{\hat{\Omega}^2 + 3}{\hat{\Omega}} \arctan \hat{\Omega} \right], \quad (45)$$

$$\phi_2(\hat{\Omega}) = \frac{1}{8\hat{\Omega}^2} \left[ 1 + \frac{\hat{\Omega}^2 - 1}{\hat{\Omega}} \arctan \hat{\Omega} \right] \quad (46)$$

(see also analogous Eq. (19) and Fig. 2 in [110]), which describe the rotational effect on turbulent convection.

From here, we obtain an estimate of the Coriolis number for solar convection in the deep layer, which should be  $\hat{\Omega} \approx 20$ . By virtue of the equations (44)-(46) and the function  $\phi_n$  (see Eq. (44)) for the value  $\hat{\Omega} \approx 20$  (see from  $0.8R_{Sun}$  in Fig. 8b<sub>2</sub>,c), the following values are adopted:

$$\phi_1 \cong 0.0171, \quad \phi_2 \cong 0.0098, \quad (47)$$

at which the radial velocity  $v_{dens}^{light}$  in Eq. (40) of toroidal field transport changes the sign at the latitude  $\theta^* = \arccos \sqrt{\phi_2/\phi_1} \cong 41^\circ$ , being negative (downward) for  $\theta > \theta^*$  and positive (upward) for  $\theta < \theta^*$ . Using Eq. (42), we find that the value of the radial velocity of toroidal field transport in the convective zone  $v_{dens}^{light}$  (see Eqs. (40)-(42)) near low latitudes (e.g.  $\theta^* = \arccos(0.985) \cong 10^\circ$ ; see also Fig. 7b) is almost identical to the value of the velocity (43), which was previously calculated using the toroidal field  $B \approx 2 \cdot 10^5$  G at  $0.8R_{Sun}$  (see Eq. (9) and Fig. 8b,c) in the  $\mathfrak{R}_{dens}(\beta, \varphi)$  (see Eq. (3.13) in [93]).

**Secondly**, we get diamagnetic pumping rate

$$v_{dia} = -\nabla \eta_T / 2 \approx 1.7 \cdot 10^2 \text{ cm/s}. \quad (48)$$

**Thirdly**, in addition to the radial profile of turbulent diffusion  $\eta_T \approx 10^{11}$  cm<sup>2</sup>/s, which is related to the diamagnetic pumping velocity  $v_{dia} \approx 1.7 \cdot 10^2$  cm/s and the distance  $2.3 \cdot 10^4$  km between  $0.8R_{Sun}$  and near  $0.85R_{Sun}$  (see the “green” line of the turbulent-toroidal magnetic field in Fig. 7b and Fig. 8b,c), we need to calculate the magnetic buoyancy velocity  $v_B$ , which is associated with a super-uniformly distributed field strength  $B \sim 2 \cdot 10^5$  G (see Fig. 7b and Fig. 8b,c). It should be remembered that for buoyant flux tubes with super-equipartition field strength  $B \sim 2 \cdot 10^5$  G  $\geq (H_p/a)^{1/2} B_{eq} \approx 3.16 B_{eq}$  with  $a \approx 0.1 H_p$ , where, as Yuhong Fan wrote (see Section 7 in [70]), “... $B_{eq} \approx 6.1 \cdot 10^4$  G is in equipartition with the kinetic energy density of the convective downflows, the magnetic buoyancy of the tubes dominates the hydrodynamic force from the convective downflows and the flux tubes can rise unaffected by convection”, but significantly affects the turbulent diamagnetic pumping!

For this, using our so-called universal van Ballegoijen-Fan-Fisher model with equations (8)-(12) with the values of the magnetic flux tube with  $\sim 2 \cdot 10^5$  G, the pressure of  $1.665 \cdot 10^{13}$  erg/cm<sup>3</sup> at  $0.8R_{Sun}$  and the rate of radiative heating  $(dQ/dt)_1 \approx 29.7$  erg · cm<sup>-3</sup> · s<sup>-1</sup>, we obtained the magnetic buoyancy velocity  $v_B \approx 1.7 \cdot 10^2$  cm/s, which, surprisingly, exactly coincides with the diamagnetic pumping velocity  $v_{dia} \approx 1.7 \cdot 10^2$  cm/s.

$$v_B \approx 1.7 \cdot 10^2 \text{ cm/s}, \quad (49)$$

which, surprisingly, exactly coincides with the diamagnetic pumping rate  $v_{dia} \approx 1.7 \cdot 10^2$  cm/s.

From here, a certain balance of three velocities,  $\vec{v}_B$ ,  $\vec{v}_{dia}$  and  $\vec{v}_{dens}$ , arises, which at  $v_B = v_{dia} \approx 1.7 \cdot$

$10^2 \text{ cm/s}$  provide both the process of blocking (via  $\vec{v}_{dens}$  at  $0.8R_{Sun}$ ) magnetic buoyancy at high latitudes

$$\uparrow v_B + \downarrow v_{dia}^{black} + \downarrow v_{dens}^{light} = \downarrow v_{dens}^{light} \cong \downarrow 4.1 \cdot 10^1 \text{ cm/s}, \quad (50)$$

and the process of raising magnetic buoyancy (via  $\vec{v}_{dens}$  at  $0.8R_{Sun}$ ) to the surface of the solar photosphere at low latitudes

$$\uparrow v_B + \downarrow v_{dia}^{black} + \uparrow v_{dens}^{light} = \uparrow v_{dens}^{light} \cong \uparrow 4.1 \cdot 10^1 \text{ cm/s}. \quad (51)$$

One of the main tasks was related to the solution of the maximum near-equatorial time  $(\tau_n)_{max}$  of the rise of the magnetic flux tube in the region between  $0.8R_{Sun}$  and near  $0.85R_{Sun}$  (see Fig. 7b and Fig. 8b,c), which is associated with the distance of turbulent diffusion  $l_{diffus} = 2.3 \cdot 10^4 \text{ km}$  and the speed of rotational  $\nabla\rho$ -pumping  $v_{dens} \approx 4.1 \cdot 10 \text{ cm/s}$ :

$$\begin{aligned} (\tau_n)_{max} &= \frac{l_{diffus}}{v_{dens}} \approx 0.56 \cdot 10^8 \text{ s} \sim 2 \text{ years}, \\ (\tau_n)_{min} &= \frac{l_{diffus}}{v_{dens}} \approx 0.56 \cdot 10^6 \text{ s} \leq 25 \text{ days}. \end{aligned} \quad (52)$$

When the toroidal fields of magnetic tubes rising from the tachocline to the solar surface, but without the participation of the turbulent diffusion distance (see Eq. 36), have strong fields of the order of  $> 2 \cdot 10^5 \text{ G}$  (see Fig. 7a and Fig. 8a), then they

$$v_B (> 2 \cdot 10^5 \text{ G}) \gg v_{dia} + v_{dens}, \quad (53)$$

suppress the existence of the velocities  $\vec{v}_{dia}$  and  $\vec{v}_{dens}$ ! This means that the near-equatorial time  $(\tau_n)_{max}$  of the magnetic flux tube rise, equal to 2 years, neglects the time of convective heating of the flux tube, which corresponds to only a few days (see analogue of  $(\tau_d)_{conv}^{max}$  in Eq. 31 and  $(\tau_d)_{conv}^{min}$  in Eq. 35).

The most interesting thing is that, in addition to the sunspots after the rise of the magnetic tube with  $B \sim 10^7 \text{ G}$  at all latitudes (see Fig. 7a and Fig. 8a) and the sunspots after the rise of the magnetic tube with  $B \leq 2 \cdot 10^5 \text{ G}$  only at low latitudes (see Fig. 7b and Fig. 8c), which are the source of the double maxima of the 11-year solar cycles (see the full experimental evidence in Section II B 2), we are interested in the problem or, more precisely, the physics of the tilt angle of Joy's law [111, 112] and how it is related to the magnetic  $\nabla\rho$ -pumping?

From here, this raises an unexpected question: In what way, in addition to the visible magnetic tube at strong fields at all latitudes (see Fig. 7a and Fig. 8a), the “invisible” magnetic tube at high latitudes (see Fig. 8b<sub>2</sub>) and the “visible” magnetic tube at low latitudes (see Fig. 8c), depending on the time  $(\tau_{rec})_2 \sim 2.5 \text{ years}$  of reconnection of the horizontal field in the tachocline (which is equal to the sum of  $(\tau_n)_{max} \approx 2 \text{ years}$  and the lifetime of sunspots ( $\leq 0.5 \text{ years}$ ) from several days to several months (see [69, 113, 114]) surprisingly, practically does

not depend on the direction in the radial plane down or up?

The answer, surprisingly, is not very simple. We know that the vertical compression (see Fig. 7a and Fig. 8b<sub>1</sub>) of the descending nearly empty anchored magnetic tube in strong fields of  $\sim 10^7 \text{ G}$  (and via convective heating  $(dQ/dt)_2$  is associated with a horizontal “stretching” or expansion of this magnetic tube near the tachocline, where the counter-movement of magnetic fields leads to the emergence of a collisionless interaction with fast (opposite) velocities  $(V_{rec})_1$  (and times  $(\tau_{rec})_1 (< 10 \text{ days})$ ) of the first part of the fast secondary (turbulent) reconnection (see Fig. 8b<sub>1</sub>). When the vertical compression leads to horizontal stronger “stretching” of the magnetic tube in weak fields of  $\geq 2 \cdot 10^5 \text{ G}$  (and through radiative heating  $(dQ/dt)_1$ , then the counter motion of magnetic fields (see  $(V_{rec})_1$  for Fig. 8b<sub>1</sub>) leads to the emergence of the second part of the secondary (turbulent) reconnection with a very slow Sweet-Parker speed  $(V_{rec})_2$  (see Fig. 8b<sub>2</sub>; also [95–100]). This means that the emerging weak fields of  $\geq 2 \cdot 10^5 \text{ G}$  at distances from  $0.80R_{Sun}$  to near  $0.85R_{Sun}$  are a remarkable source of rotating magnetic  $\nabla\rho$ -pumping with the rise time of the magnetic tube  $(\tau_n)_{max} \sim 2.0 \text{ years}$  from the tachocline to the solar surface (see Fig. 8c), and the lifetime of sunspots ( $\leq 0.5 \text{ years}$ ), and consequently, the time of the magnetic tube evaporation  $(\tau_{rec})_2 \leq 2.5 \text{ years}$  and their disappearance on the solar surface.

Since the study of the tendency of the tilt angle of Joy's law is very important for understanding the evolution of the solar magnetic field, then unlike the heavy calculations of theoretical estimates of the averaged angle tilt of sunspots with increasing latitude, we can summarize our results (see Eqs. (5)-(9) in [113]), which can simultaneously be expressed in the form of simple and understandable physics of Joy's law. It is known that, according to [113] and [69], the Coriolis force is proportional to the magnetic buoyancy velocity  $v_B$ , which can be estimated taking into account the balance between the buoyancy force (the term on the left) and the drag force (left term) and the drag force (right term):

$$\frac{B^2}{8\pi H_p} = C_D \frac{\rho_{ext} v_B^2}{\pi a}, \quad (54)$$

where the buoyancy velocity  $v_B$  is related to the radius  $a$  of the cross-section of the magnetic tube.

Taking into account Eqs. (18) and (19) by [114] and using the theoretical values of the tilt angle  $\alpha$ , the latitude angle  $\theta$  and the radial parameter  $\xi = r/R_{Sun} \sim 0.80$ , one can easily obtain a simplified equation in the following form:

$$\sin(\text{tilt}) \propto \frac{\sqrt{a(\xi, \theta)}}{B} \sin(\text{latitude}). \quad (55)$$

This means that looking at equation (55), we understand that when magnetic tubes contain relatively large radii  $a$  (due to radiative heat transfer  $(dQ/dt)_1$  (see

Fig. 8b<sub>2,c</sub>) and low magnetic fields ( $\leq 10^5 G$ ), then the tilt angle of Joy's law are born from here, and when magnetic tubes have practically zero radii  $a$  (due to convective heat transfer  $(dQ/dt)_2$  (see Fig. 8b<sub>2,c</sub>) and strong high magnetic fields ( $> 10^5 G$ ), then the tilt angle of Joy's law disappears!

It can be said in a completely different way. If radiative heat transfer  $(dQ/dt)_1$  (see Fig. 8b<sub>2,c</sub>) or the presence of magnetic  $\nabla\rho$ -pumping is used in magnetic tubes, then, as usual, the tilt angles of Joy's law appear in sunspots, when convective heat transfer  $(dQ/dt)_2$  or the disappearance of magnetic  $\nabla\rho$ -pumping (see Fig. 8b<sub>2,c</sub>) is used in magnetic tubes, then, strangely enough, the tilt angles of Joy's law disappear in sunspots!

In this regard, we are interested in an intriguing question: Where and how do sunspots appear, in which, according to [115], the maxima of the double peak in the sunspot cycle appear? And how does the first maximum – the maximum number of spots – physically differ from the second – the maximum of large spots?

Below we will show that, firstly, the first maximum differs from the second maximum by being shifted in time by 2 years (see text after Eq. (53)) later than the main (first!) maximum of the solar activity cycle. Secondly, according to equation (54), when the flux tube has a large radius and a low magnetic field, then this magnetic tube, surprisingly, is the source of the formation of the tilt angle (via the Coriolis force, and not necessarily on the surface of the photosphere (see Fig. 8c)) and a large area of the spot on the surface of the Sun. Conversely, when the flux tube has a small radius and a high magnetic field, then the magnetic tube, on the one hand, is not connected to the source of the formation of the tilt angle of Joy's law (through the Coriolis force), and on the other hand, surprisingly, has a small spot area on the surface of the Sun.

This raises a second intriguing point. One of the first solutions in our section is secondary reconnection of the MFT, which involves a turbulent diffusivity of  $10^{11} cm/s$  and a tilt angle of Joy's law between magnetic fields ranging from  $2 \cdot 10^5 G$  (at  $0.8R_{Sun}$ ) to  $6 \cdot 10^4 G$  (at  $0.85R_{Sun}$ ). Moreover, due to the relationship between turbulent diffusivity and the tilt angle of Joy's law, the direction of magnetic  $\nabla\rho$ -pumping (upward or downward (see Fig. 8b<sub>2,c</sub>)) is sensitive to the sign of the multiplier in equations (45)-(45), which depends on the polar angle (co-latitude) and the behavior of the Coriolis number functions in the convective zone.

It is crucial that the existence of secondary MFT reconnection generates a secondary maximum in the 11-year sunspot cycle. This is because when the primary reconnection, in which the buoyancy of a practically empty magnetic flux tube at  $\sim 10^7 G$  rises from the tachocline to the photosphere for  $\sim 2$  to 10 days, transitions to secondary reconnection, the latter is associated with a buoyancy of practically MFT from  $\sim 6 \cdot 10^4 G$  from  $0.85R_{Sun}$  (see Fig. 8c)) to the photosphere. From this we understand that since the lifetime of  $\sim 2$  years for the rotating

magnetic  $\nabla\rho$ -pumping from  $2 \cdot 10^5 G$  at  $0.8R_{Sun}$  (see Fig. 8c) to  $6 \cdot 10^4 G$  is related to the lifetime of the order of  $\sim 10$  days for the buoyancy of almost MFT from  $\sim 6 \cdot 10^4 G$  to the photosphere, this means that the secondary reconnection of MFT from the tachocline to the photosphere is also equal to  $\sim 2$  years.

In other words, the connection between primary and secondary reconnections (or first and second maxima) is the connection of MFTs between lifetimes of the order of  $\sim 2$  to 10 days and lifetimes of the order of  $\sim 2$  years, which is preserved by 11-year sunspot cycles without any dynamo.

## 2. Double maxima of 11-year sunspot cycles and the Gnevyshev gap

The phenomenon of a double peak in the sunspot cycle was discovered by Mstislav Gnevyshev in 1963 [115] during a study of coronal emission and areas of active formations in the 11-year cycle 19 [115]. First, Gnevyshev analyzed the evolution of the annual average intensity of the green coronal spectral line  $\lambda 530.3$  (which serves as a direct indicator of magnetic activity and coronal heating) in five-degree heliolatitude intervals during the cycle 19 and discovered two maxima in the intensity of the corona. According to data in [116–118], the first maximum of the area of sunspot groups coincides with the main maximum of the 11-year cycle for Wolf numbers, while the second maximum is associated with an increase in the number of large sunspots (the so-called maximum of sunspot intensities) [119, 120]. In other words, the first maximum is the maximum in the number of sunspots, and the second is the maximum of large sunspots [120]. The more large spots in the cycle, the more distinct the two peaks. These features were later confirmed and for the cycle 20 (see Fig. 9), including for the solar northern and southern hemispheres separately [115].

In contrast to the “new solar dynamo era” (see e.g. [1, 2, 70, 80, 121–124]), we used our alternative theory of magnetic flux tubes at strong fields via photons of axion origin. The essence of double maximum 11-year sunspot cycles, the source of which is the generation of a magnetic field near the bottom of the convective zone and the subsequent rise of the field from the deep layers to the surface in the photosphere, manifests itself at strong fields only (see Fig. 8a, Fig. 8b<sub>2,c</sub>). This means that the two maxima are related as follows: the first maximum (the primary reconnection of the empty MFT with  $10^7 G$  at  $0.72R_{Sun}$ ; see Figs. 7a, 8a), which generates a very “fast” velocity to the solar surface (on the order of several days; see Eq. (31)  $\sim 1 - 2 days$ ) is transformed into a secondary maximum (the secondary reconnection of the empty MFT with  $10^6 G$  at  $0.85R_{Sun}$ ; see Figs. 7a, 8a), which then generates a “very slow” velocity to the solar surface (on the order of two years; see Eq. (52) of  $(\tau_n)_{max} \sim 2.0 years$  for Fig. 8b<sub>2,c</sub>).

In other words, the “very slow” second maximum de-

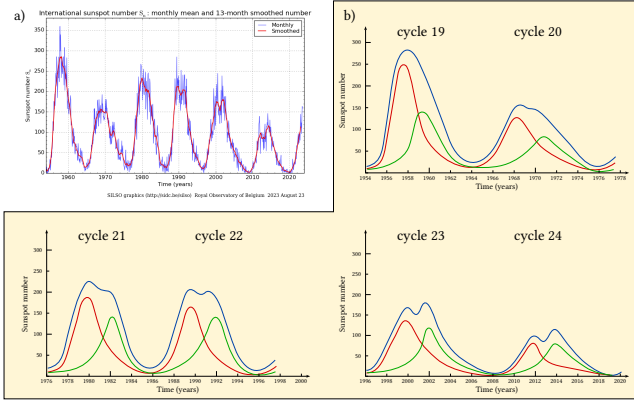


FIG. 9. Variation in the number of sunspots for six cycles from 19 to 24 associated with double maxima of 11-year solar cycles: (a) solid red lines of sunspot cycles – smoothed values (<https://sidc.be/SILSO>) Royal Observatory of Belgium 2023, August 23. (b) theoretical assessment of double maxima of 11-year solar cycles: solid line – “smoothed” blue values of sunspot cycles, in which the sum of the curves with the first maximum in the form of a “red” value and the second maximum in the form of a “green” value almost exactly coincides with a solid “blue” line of the corresponding cycle.

depends only on two interrelated causes: the very slow secondary reconnection (see Fig. 8b<sub>2,c</sub>) of the magnetic flux tube, which depends both at a strong magnetic field of  $> 2 \cdot 10^5 G$ , having two sections between  $0.7R_{Sun}$  and near  $0.80R_{Sun}$ , and between  $0.85R_{Sun}$  and the photosphere (see Fig. 8b<sub>2,c</sub>), and, surprisingly, at a weak magnetic field of  $< 2 \cdot 10^5 G$ , where the so-called effects of turbulent diamagnetic transport and rotating  $\nabla\rho$ -pumping appear for the first time, which provide both the process of blocking magnetic buoyancy at high latitudes (see Fig. 8b<sub>2</sub>), and at near-equatorial latitudes predetermines the process of dominance of the Coriolis force with rotating  $\nabla\rho$ -pumping with  $< 2 \cdot 10^5 G$  at a distance  $2.3 \cdot 10^4 km$  between  $0.80R_{Sun}$  and near  $0.85R_{Sun}$  (see Fig. 8c), which ultimately generates a “shift” of the arcuate ascending loop in the form of the tilt angle of Joy’s law on the solar surface (see Fig. 8c).

In this case, the key role in the proposed mechanism of double maxima is played by two “waves” of toroidal fields, in which the first wave, with a strong field of  $\sim 10^7 G$  and without the participation of secondary reconnection, first arises at all latitudes, and then, as a consequence, instead of the first wave, a second wave appears with a weak magnetic field of  $< 2 \cdot 10^5 G$  between  $0.80R_{Sun}$  and  $0.85R_{Sun}$ , which is obtained from the same primary wave, but with the participation of secondary reconnection, only at the latitudes of the equatorial surface of the Sun.

That is to say, the first maximum is the maximum of the number of spots that are sources of the magnetic flux tube (anchored in the overshoot tachocline) with  $B \sim 10^7 G$  and with the participation of primary re-

connection (see Fig. 3 and Fig. 4a; also Fig. 7a), and the second maximum is the maximum of large spots that are the result of the appearance of magnetic flux tubes with  $B \sim 10^7 G$  and with the participation of secondary reconnection (see Fig. 4b and Fig. 8b<sub>2,c</sub>). From here, we are interested, in fact, in the very important secondary magnetic reconnection (see Fig. 7b and Fig. 8b<sub>2,c</sub>) during the rise of the magnetic flux tube in the solar photosphere, which is one of the two sources of the observed double maxima of one sunspot cycle – it shifts by  $\sim 2.5 years$  between the primary (see the “red” curves in Fig. 9b) and secondary (see the “green” curves in Fig. 9b) sunspot maxima (see “smoothed” blue curves in Fig. 9b). Moreover, it is the secondary maximum of sunspots that is also associated with both observational data of the tilt angle of Joy’s law (see Fig. 8c from the right) and with the disappearance of sunspots on the surface of the Sun (see Fig. 4c,d).

And finally, we realize that the observed double maxima, for example in cycles 19-24 (see Fig. 9a), also have different ratios between the numbers of very “fast” primary maxima ( $(S_n)_{max}^{primary}$ ) (see the red curves in Fig. 9b; also Fig. 7a and Fig. 8a) and very “slow” secondary maxima (see the “green” curves in Fig. 9b)

$$(S_n)_{max}^{primary} / (S_n)_{max}^{secondary} \approx \begin{cases} 2 & \text{at } \sim 300 \text{ sunspots} \\ 1.5 & \text{at } \sim 150 \div 200 \\ 1 & \text{at } \sim 100 \text{ sunspots} \end{cases} \quad (56)$$

and at the same time have almost the same difference between the secondary reconnection time  $(\tau_{rec})_2 \leq 2.5 years$  of the horizontal field in the tachocline (which is equal to the sum of  $(\tau_n)_{max} \approx 2$  and the lifetime of sunspots ( $\leq 0.5 years$ ) from several days to several months (see [83, 101]), which shift by  $\sim 2.0 years$ ,

$$(\tau_n)_{max} = (\tau_{rec})_{max}^{secondary} - (\tau_{rec})_{max}^{primary} \sim 2.0 years \quad (57)$$

between the “experimental” data of double sunspot maxima – very “slow” second maxima  $(\tau_{rec})_{max}^{secondary}$  and very “fast” primary maxima  $(\tau_{rec})_{max}^{primary}$  (see Fig. 9b).

This raises a valid question: How is the unique source of the butterfly diagram found only in the form of 11-year variations in sunspot numbers or only in the form of alternating 22-year fundamental cycles of solar activity?

Here we show that, as expected, the source of the butterfly diagram is found only in the 11-year variations of the sunspot numbers (see [117]). Below we present an understanding of the so-called latitude-time interval (or gap) between nearby butterflies by the remarkable solar physicist Gnevyshev [117].

To understand the physics of the Gnevyshev gap, we need to briefly describe the solution of the following interrelated problems:

- First, these are 11-year variations of sunspots (see [14]). A unique result of our model is the fact that the 11-year periods, velocities and modulations of the S102 star (see Fig. 6b in [14]) near the

black hole are a significant indicator of the density modulation of the ADM halo in the fundamental plane of the Galactic center, which closely correlates with the density modulation of baryonic matter near the SMBH. If the ADM halo modulations in the GC black hole lead to ADM density modulations on the solar surface (via vertical density waves between the disk and the black hole to the solar neighborhood), then there is an “experimental” anticorrelation identity between such indicators as the 11-year ADM density modulation in the solar interior and the modulations of solar axions (or photons of axion origin), and equivalently between the modulations of solar axions (or photons of axion origin) and the sunspot cycles!

- Secondly, we know why we never see sunspots at the solar poles. The answer is quite simple. We know that both the tilt angle between the geometric and magnetic meridians, which are tilted by 7.25 degrees relative to the ecliptic, and the magnetic field of the northern (or southern) part of the meridional circulation, which radially corresponds to a length of about  $\sim 22^\circ$ , add up to about  $\sim 30^\circ$ . It follows clearly from this that the magnetic field of the meridional circulation part will always slow down the magnetic field of the flux tube, which will almost never rise to the surface of the photosphere. This means that the magnetic fields of the flux tubes will only appear below about  $90^\circ - 30^\circ \approx 60^\circ$  at high latitudes. And that is precisely why no one observes sunspots at the poles of the Sun above  $60^\circ$ !
- And Thirdly, we can finally observe (see Fig. 6a of [14] for Japanese x-ray telescope Yohkoh (1991–2001)) and obtain the physics of photons of axion origin, which are associated with primary reconnection, only in those sunspots which are practically independent of the differential rotation of the Sun (when the equator rotates faster than the poles) in the butterfly diagram. Clearly, in other sunspots which depend exactly on secondary reconnection of magnetic flux tubes and, as a consequence, on the tilt angle of Joy’s law on the surface of the Sun (see Fig. 8c), there can never be occurrences of axion origin photons in sunspots due to the differential rotation of the Sun.

From here we now return to the physics of the Gnevyshev gap. The answer is quite simple. The Gnevyshev intervals in the butterfly diagrams are related to the 11-year modulations of the ADM density, trapped on the Sun (via vertical density waves from the disk to the solar neighborhood) and, as a result, to anticorrelated indicators of variations in the sunspot cycles or photons of axion origin. When the ADM density in the solar interior is low (or the sunspot count is high), then the Gnevyshev intervals will be short in time. Conversely, when the ADM density in the solar interior is high (or the sunspot

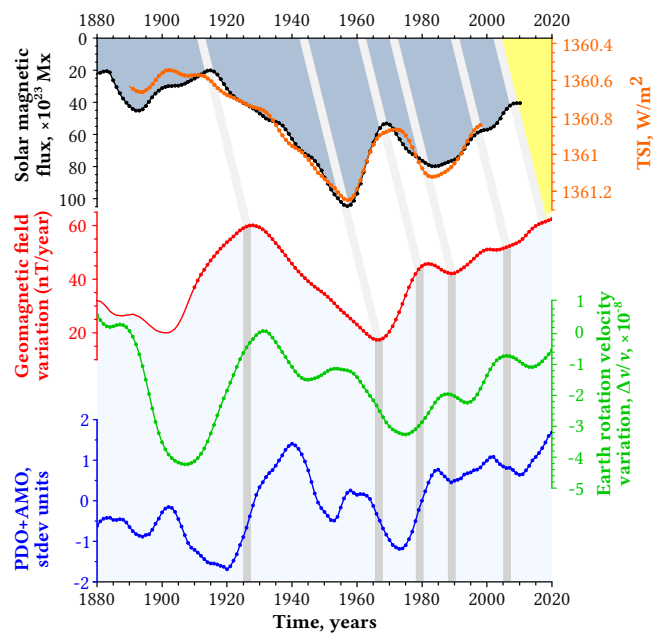


FIG. 10. The time variations of total solar irradiance (TSI; orange curve; see Fig. 9 in [125]), simulated solar magnetic flux (black curve; see Fig. 7 in [126]; and also Fig. 16 in [127]) (both curves were smoothed with 29-year weighted moving average); the geomagnetic field secular variations (the Y-component; red curve) measured at the Eskdalemuir observatory [128]; variations in the Earth’s rotation speed (green curve; joined data from Fig. 3 in [129], Fig. 3.9 in [130], and the EOP C01 IAU1980 (1846–now) dataset [131]); the variations of the average global ocean level (Pacific Decadal Oscillation (PDO) [132] + Atlantic Multidecadal Oscillation (AMO) [133]; blue curve) with a trend in mm/years near 60-year oscillation (see Fig. 1 in [134]). The latter three curves were first smoothed using 5-year moving average, and then the 11-year moving average. All considered time variations between the Sun and the Earth always have a time interval of approximately  $\sim 10 \div 11$  years. The only serious disagreements between the reconstructions and observations occur during the Second World War, especially in the period 1944–1945 (see [135]).

count is low), then the Gnevyshev intervals will be longer in time. As no surprisingly, it is the presence of ADM density modulations that shows that the appearance of “our indicated” Gnevyshev gap is the result of precisely 11-year variations of butterfly cycles with sunspots.

The most interesting thing is that it is the 11-year variations of sunspot cycles or photons of axion origin (see Figs. 5a and 6b in [14]) that are anticorrelated not only with the 11-year modulations of ADM density on the Sun, but also with the 11-year modulations of ADM density in the solar neighborhood, and, in particular, on Earth (see e.g. Fig. 10).

First, we recall that the physics of experimental data related to the anticorrelation between 11-year variations in the luminosity of the Sun and the Earth (see Fig. 10)

currently cannot explain one of the most mystical phenomena of solar-terrestrial physics, which is contained in well-known experiments, for example, between the temporal variations of the magnetic flux of the solar tachocline (black curve; see [126] and Fig. 16 in [127]), and secular variations in the Earth's magnetic field (Y-component from [128]), or variations in the Earth's rotation speed (see [129, 130]), as well as the variations in the mean global sea level (Pacific Decadal Oscillation (PDO) [132] + Atlantic Multidecadal Oscillation (AMO) [133]) with a trend in mm/years near 60-year oscillation (see Fig. 1 in [134]), between which there is a time lag of about 10-11 years, respectively (see Fig. 10;

and also Fig. 6 in [14].

### III. SUMMARY AND OUTLOOK

Most importantly, the existing void in the tube causes high velocities and short lifetimes of sunspots from the tachocline to the photosphere, which is consistent with experimental data. This means that the modernity of a well-developed helioseismological inversion, surprisingly, persists to this day.

The perspective is to understand the physics of the anticorrelation between 11-year variations of total solar irradiance and 11-year variations of the magnetic field and other Earth parameters (see Fig. 10).

- 
- [1] P. Charbonneau and D. Sokoloff, *Space Science Reviews* **219**, 35 (2023).
- [2] P. J. Käpylä, M. K. Browning, A. S. Brun, G. Guerrero, and J. Warnecke, *Space Science Reviews* **219**, 58 (2023).
- [3] G. G. Dahlquist, *BIT* **3**, 27–43 (1963).
- [4] E. N. Parker, *Space Sci. Rev.* **122**, 15 (2009).
- [5] M. Rempel and R. Schlichenmaier, *Living Rev. Solar Phys.* **8** (2011).
- [6] E. N. Parker, *Astrophys. J.* **121**, 491 (1955).
- [7] L. Biermann, *Vierteljahrsschrift Astron. Gesellschaft.* **76**, 194 (1941).
- [8] E. N. Parker, *Astrophys. J.* **230**, 905 (1979).
- [9] H. Alfvén, *Nature* **150**, 405 (1942).
- [10] E. N. Parker, *Astrophysical Journal* **189**, 563 (1974).
- [11] E. N. Parker, *Astrophysical Journal* **190**, 429 (1974).
- [12] E. N. Parker, *Solar Physics* **36**, 249–274 (1974).
- [13] E. N. Parker, *Astrophysical Journal* **215**, 370 (1977).
- [14] V. D. Rusov, I. V. Sharph, V. P. Smolyar, M. V. Einhorn, and M. E. Beglaryan, *Physics of the Dark Universe* **31**, 100746 (2021).
- [15] E. E. Deluca and P. A. Gilman, *Geophysical & Astrophysical Fluid Dynamics* **37**, 85 (1986).
- [16] A. V. Ettingshausen and W. Nernst, *Wied. Ann.* **29**, 343 (1886).
- [17] E. H. Sondheimer, *Proceedings of the Royal Society of London. Series A, Mathematical and Physical Sciences* **193**, 484 (1948).
- [18] L. J. Spitzer, *Physics of Fully Ionized Gases*, 2nd ed. (Dover Publications, Inc., Mineola, New York, 2006).
- [19] Y. B. Kim and M. J. Stephen, in *Superconductivity*, Vol. 2, edited by R. Parks (Dekker, New York, 1969).
- [20] Let us remind from where the fairly young S-stars (Fig. 8a in [14]) appear in our galaxy between the black hole and the disk. Since we know that in our galaxy, in addition to the supermassive black hole (SMBH), there is the so-called intermediate black hole (IMBH; see evidence [136]). If we take into account the evolution of binary SMBH-IMBH, then when one body (SMBH) exchanges partners of binary stars orbiting the IMBH (Fig. 8b in [14]), and through the extreme gravitational-tidal field, one star is captured (SMBH) and loses energy, while the other escapes, receives all this energy and, due to the hypervelocity of B-type stars – the IMBH sling (Fig. 8b in [14]), simply flies out of the galaxy. From here it becomes clear how in other galaxies a young S-star can end up between a black hole and a disk.
- [21] G. G. Raffelt, *Phys. Lett.* **592**, 391 (2004).
- [22] G. G. Raffelt, *Lect. Notes Phys.* **741**, 51 (2008), [arXiv:hep-ph/0611350](https://arxiv.org/abs/hep-ph/0611350).
- [23] A. Caputo and G. Raffelt, in *Proceedings of 1st General Meeting and 1st Training School of the COST Action COSMIC WISPerS — PoS(COSMICWISPerS)* (Sissa Medialab, Bari and Lecce, Italy, 2024) p. 041.
- [24] C. O'Hare, *Cosmology of axion dark matter*, in *Proceedings of 1st General Meeting and 1st Training School of the COST Action COSMIC WISPerS — PoS(COSMICWISPerS)*, Vol. 454 (SISSA Medialab, 2024) p. 040.
- [25] R. D. Peccei and H. R. Quinn, *Physical Review Letters* **38**, 1440–1443 (1977).
- [26] R. D. Peccei and H. R. Quinn, *Phys. Rev. D* **16**, 1791 (1977).
- [27] F. Wilczek, *Phys. Rev. Lett.* **40**, 279 (1978).
- [28] S. Weinberg, *Physical Review Letters* **40**, 223–226 (1978).
- [29] J. Preskill, M. B. Wise, and F. Wilczek, *Physics Letters B* **120**, 127 (1983).
- [30] L. Abbott and P. Sikivie, *Physics Letters B* **120**, 133 (1983).
- [31] M. Dine and W. Fischler, *Physics Letters B* **120**, 137 (1983).
- [32] A. Ayala, I. Domínguez, M. Giannotti, A. Mirizzi, and O. Straniero, *Phys. Rev. Lett.* **113**, 191302 (2014).
- [33] M. Buschmann, R. T. Co, C. Dessert, and B. R. Safdi, *Phys. Rev. Lett.* **126**, 021102 (2021).
- [34] P. Carenza, T. Fischer, M. Giannotti, G. Guo, G. Martínez-Pinedo, and A. Mirizzi, *Journal of Cosmology and Astroparticle Physics* **2019** (10), 016–016.
- [35] P. Carenza, B. Fore, M. Giannotti, A. Mirizzi, and S. Reddy, *Phys. Rev. Lett.* **126**, 071102 (2021).
- [36] CAST Collaboration, *Nature Physics* **13**, 584–590 (2017).
- [37] S. J. Asztalos, G. Carosi, C. Hagmann, D. Kinion, K. van Bibber, J. Hoskins, J. Hwang, P. Sikivie, D. B. Tanner, R. Bradley, and J. Clarke, *Phys. Rev. Lett.* **104**,

- 041301 (2010).
- [38] W. U. Wuensch, S. D. Panfilis-Wuensch, Y. K. Semertzidis, J. T. Rogers, A. C. Melissinos, H. J. Halama, B. E. Moskowitz, A. G. Prodel, W. B. Fowler, and F. A. Nezrick, *Phys. Rev. D* **40**, 3153 (1989).
- [39] B. M. Brubaker, L. Zhong, S. K. Lamoreaux, K. W. Lehnert, and K. A. van Bibber, *Physical Review D* **96**, 123008 (2017).
- [40] L. Zhong, S. Al Kenany, K. M. Backes, B. M. Brubaker, S. B. Cahn, G. Carosi, Y. V. Gurevich, W. F. Kindel, S. K. Lamoreaux, K. W. Lehnert, S. M. Lewis, M. Malnou, R. H. Maruyama, D. A. Palken, N. M. Rapidis, J. R. Root, M. Simanovskaia, T. M. Shokair, D. H. Speller, I. Urdinaran, and K. A. van Bibber, *Phys. Rev. D* **97**, 092001 (2018).
- [41] T. Braine, R. Cervantes, N. Crisosto, N. Du, S. Kimes, L. J. Rosenberg, G. Rybka, J. Yang, D. Bowring, A. S. Chou, R. Khatiwada, A. Sonnenschein, W. Wester, G. Carosi, N. Woollett, L. D. Duffy, R. Bradley, C. Boutan, M. Jones, B. H. LaRoque, N. S. Oblath, M. S. Taubman, J. Clarke, A. Dove, A. Eddins, S. R. O’Kelley, S. Nawaz, I. Siddiqi, N. Stevenson, A. Agrawal, A. V. Dixit, J. R. Gleason, S. Jois, P. Sikivie, J. A. Solomon, N. S. Sullivan, D. B. Tanner, E. Lentz, E. J. Daw, J. H. Buckley, P. M. Harrington, E. A. Henriksen, and K. W. Murch (ADMX Collaboration), *Phys. Rev. Lett.* **124**, 101303 (2020).
- [42] S. Lee, S. Ahn, J. Choi, B. R. Ko, and Y. K. Semertzidis, *Phys. Rev. Lett.* **124**, 101802 (2020).
- [43] K. M. Backes, D. A. Palken, S. A. Kenany, B. M. Brubaker, S. B. Cahn, A. Droster, G. C. Hilton, S. Ghosh, H. Jackson, S. K. Lamoreaux, and et al., *Nature* **590**, 238 (2021).
- [44] G. G. Raffelt, Astrophysical axion bounds, in *Axions: Theory, Cosmology, and Experimental Searches*, edited by M. Kuster, G. Raffelt, and B. Beltrán (Springer Berlin Heidelberg, Berlin, Heidelberg, 2008) pp. 51–71.
- [45] G. Carosi, A. Friedland, M. Giannotti, M. Pivovarov, J. Ruz, and J. Vogel (2013), [arXiv:1309.7035](https://arxiv.org/abs/1309.7035).
- [46] J. E. Kim, *Phys. Rev. Lett.* **43**, 103 (1979).
- [47] M. Shifman, A. Vainshtein, and V. Zakharov, *Nucl. Phys. B* **166**, 493 (1980).
- [48] A. Friedland, M. Giannotti, and M. Wise, *Phys. Rev. Lett.* **110**, 061101 (2013).
- [49] J. Bahcall and M. Pinsonneault, *Rev. Mod. Phys.* **64**, 885 (1992).
- [50] A. Kolmogorov, *Akademiia Nauk SSSR Doklady* **30**, 301 (1941).
- [51] A. N. Kolmogorov, *Soviet Physics Uspekhi* **10**, 734 (1968).
- [52] E. N. Parker, *The Astrophysics Journal* **433**, 867 (1994).
- [53] H. C. Spruit, A. M. Title, and A. A. Van Ballegoijen, *Solar Physics* **110**, 115 (1987).
- [54] P. R. Wilson, P. S. McIntosh, and H. B. Snodgrass, *Solar Physics* **127**, 1 (1990).
- [55] E. N. Parker, *Astrophysical Journal* **198**, 205 (1975).
- [56] E. N. Parker, *Cosmical magnetic fields: Their origin and their activity* (Oxford, Clarendon Press, 1979) p. 858.
- [57] A. A. van Ballegoijen, *Astronomy and Astrophysics* **113**, 99 (1982).
- [58] E. Böhm-Vitense, *Zeitschrift fuer Astrophysik* **46**, 108 (1958).
- [59] H. C. Spruit, *Magnetic Flux Tubes and Transport of Heat*, Ph.D. thesis, Ph. D. Thesis, Utrecht University (1977).
- [60] A. S. Brun, M. S. Miesch, and J. Toomre, *The Astrophysical Journal* **742**, 79 (2011).
- [61] H. Spruit, *Solar Physics* **34**, 277 (1974).
- [62] J. Christensen-Dalsgaard, M. J. P. F. G. Monteiro, and M. J. Thompson, *Monthly Notices of the Royal Astronomical Society* **276**, 283 (1995).
- [63] J. Christensen-Dalsgaard, M. J. P. F. G. Monteiro, M. Rempel, and M. J. Thompson, *Monthly Notices of the Royal Astronomical Society* **414**, 1158 (2011).
- [64] Y. Fan and G. Fisher, *Solar Phys.* **166**, 17 (1996).
- [65] H. C. Spruit and A. A. van Ballegoijen, *Astronomy and Astrophysics* **106**, 58 (1982).
- [66] S. Z. Ali and S. Dey, *Physics of Fluids* **32**, 121401 (2020).
- [67] M. A. Weber and Y. Fan, *Solar Physics* **290**, 1295 (2015), [arXiv:1503.08034](https://arxiv.org/abs/1503.08034) [astro-ph.SR].
- [68] M. A. Weber and M. K. Browning, *The Astrophysical Journal* **827**, 95 (2016).
- [69] Y. Fan, G. H. Fisher, and E. E. Deluca, *Astrophysical Journal* **405**, 390 (1993).
- [70] Y. Fan, *Living Reviews in Solar Physics* **18**, 5 (2021).
- [71] K. L. Harvey, *Magnetic bipoles on the Sun*, Ph.D. thesis, University of Utrecht, Netherlands (1993).
- [72] N. R. Sheeley and J. W. Harvey, *Solar Physics* **70**, 237–249 (1981).
- [73] J. E. Bailey, G. A. Rochau, R. C. Mancini, C. A. Iglesias, J. J. Macfarlane, I. E. Golovkin, C. Blancard, P. Cosse, and G. Faussurier, *Physics of Plasmas* **16**, 058101 (2009).
- [74] S. Ilonidis, J. Zhao, and A. Kosovichev, *Science* **336**, 296 (2012).
- [75] S. Ilonidis, J. Zhao, and T. Hartlep, *The Astrophysical Journal* **777**, 138 (2013).
- [76] A. G. Kosovichev, J. Zhao, and S. Ilonidis, *ArXiv e-prints* (2016), [arXiv:1607.04987](https://arxiv.org/abs/1607.04987) [astro-ph.SR].
- [77] A. G. Kosovichev, J. Zhao, and S. Ilonidis, Local helioseismology of emerging active region: A case study, in *Variability of the Sun and Sun-like Stars: from Asteroseismology to Space Weather* (EDP Sciences, Les Ulis, 2018) pp. 15–38.
- [78] A. C. Birch, H. Schunker, D. C. Braun, R. Cameron, L. Gizon, B. Löptien, and M. Rempel, *Science Advances* **2**, 10.1126/sciadv.1600557 (2016).
- [79] S. Jabbari, A. Brandenburg, D. Mitra, N. Kleeorin, and I. Rogachevskii, *Monthly Notices of the Royal Astronomical Society* **459**, 4046 (2016).
- [80] V. N. Krivodubskij, *Astronomische Nachrichten* **326**, 61 (2005).
- [81] V. N. Krivodubskij, *Advances in Space Research* **68**, 3943 (2021).
- [82] V. N. Krivodubskii, *Soviet Astronomy* **36**, 432 (1992).
- [83] K. Petrovay and L. van Driel-Gesztelyi, *Solar Physics* **176**, 249 (1997).
- [84] L. L. Kichatinov, *Astronomy and Astrophysics* **243**, 483 (1991).
- [85] Y. B. Zel’dovich, *Sov. Phys. JETP* **4**, 460 (1957).
- [86] Y. B. Zel’dovich, *Sov. Phys. JETP* **31**, 154 (1956).
- [87] L. J. Spitzer, *The Astrophysical Journal* **125**, 525 (1957).
- [88] L. L. Kichatinov and G. Rüdiger, *Astronomische Nachrichten* **329**, 372 (2008).
- [89] H. Köhler, *Astronomy and Astrophysics* **25**, 467 (1973).
- [90] K.-H. Rädler, *Zeitschrift für Naturforschung A* **23**, 1841

- (1968).
- [91] K.-H. Rädler, *Zeitschrift für Naturforschung A* **23**, 1841 (1968).
- [92] F. Krause and K.-H. Raedler, *Organic Photonics and Photovoltaics* (Pergamon Press, 1980).
- [93] L. L. Kichatinov and G. Ruediger, *Astronomy and Astrophysics* **260**, 494 (1992).
- [94] F. Chen, M. Rempel, and Y. Fan, *The Astrophysical Journal* **937**, 91 (2022).
- [95] A. Lazarian and E. T. Vishniac, *The Astrophysical Journal* **517**, 700 (1999).
- [96] A. Lazarian, E. T. Vishniac, and J. Cho, *The Astrophysical Journal* **603**, 180 (2004).
- [97] G. Kowal, A. Lazarian, E. T. Vishniac, and K. Otmianowska-Mazur, *The Astrophysical Journal* **700**, 63 (2009).
- [98] A. Lazarian, G. L. Eyink, A. Jafari, G. Kowal, H. Li, S. Xu, and E. T. Vishniac, *Physics of Plasmas* **27**, 012305 (2020).
- [99] E. N. Parker, *Proceedings of the National Academy of Sciences* **43**, 8–14 (1957).
- [100] P. A. Sweet, in *Electromagnetic Phenomena in Cosmical Physics*, IAU Symposium, Vol. 6, edited by B. Lehnert (1958) p. 123.
- [101] S. K. Solanki, *The Astronomy and Astrophysics Review* **11**, 153 (2003).
- [102] L. L. Kichatinov, *Geophysical & Astrophysical Fluid Dynamics* **38**, 273–292 (1987).
- [103] M. Stix, *The Sun*, Astronomy and Astrophysics Library (Springer Berlin Heidelberg, Berlin, Heidelberg, 2002).
- [104] R. Kippenhahn, A. Weigert, and A. Weiss, *Stellar Structure and Evolution*, Astronomy and Astrophysics Library (Springer Berlin Heidelberg, Berlin, Heidelberg, 2012).
- [105] J. Schumacher and K. R. Sreenivasan, *Rev. Mod. Phys.* **92**, 041001 (2020).
- [106] P. Bradshaw, *Nature* **249**, 135 (1974).
- [107] D. O. Gough, *Astrophysical Journal* **214**, 196 (1977).
- [108] D. Gough, in *Problems of Stellar Convection*, Lecture Notes in Physics, Berlin Springer Verlag, Vol. 71, edited by E. A. Spiegel and J.-P. Zahn (1977).
- [109] S. I. Vainshtein and L. L. Kichatinov, *Geophysical & Astrophysical Fluid Dynamics* **24**, 273 (1983).
- [110] L. L. Kichatinov and A. A. Nepomnyashchikh, *Advances in Space Research* **58**, 1554 (2016), solar Dynamo Frontiers.
- [111] V. G. Ivanov, *Geomagnetism and Aeronomy* **52**, 999 (2012).
- [112] M. Dasi-Espuig, S. K. Solanki, N. A. Krivova, R. Cameron, and T. Peñuela, *Astronomy and Astrophysics* **518**, A7 (2010), arXiv:1005.1774 [astro-ph.SR].
- [113] S. D’Silva and A. R. Choudhuri, *Astronomy and Astrophysics* **272**, 621 (1993).
- [114] Y. Fan, G. H. Fisher, and A. N. McClymont, *Astrophysical Journal* **436**, 907 (1994).
- [115] M. N. Gnevyshev, *Soviet Astronomy* **7**, 311 (1963).
- [116] A. Antalova and M. N. Gnevyshev, *Soviet Astronomy* **9**, 198 (1965).
- [117] M. N. Gnevyshev, *Solar Physics* **1**, 107 (1967).
- [118] M. N. Gnevyshev, *Solar Physics* **51**, 175 (1977).
- [119] Y. I. Vitinskij, M. Kopetskij, and G. V. Kuklin, *Statistics of the spot-forming activity of the sun.* (1986) (in Russian).
- [120] M. Kopecký and G. V. Kuklin, *Bulletin of the Astronomical Institutes of Czechoslovakia* **20**, 22 (1969).
- [121] Z. Zhang and J. Jiang, *The Astrophysical Journal* **930**, 30 (2022).
- [122] Z. Zhang, J. Jiang, and H. Zhang, in *The Era of Multi-Messenger Solar Physics*, IAU Symposium, Vol. 372, edited by G. Cauzzi and A. Tritschler (2023) pp. 91–93.
- [123] G. M. Vasil, D. Lecoanet, K. Augustson, K. J. Burns, J. S. Oishi, B. P. Brown, N. Brummell, and K. Julien, *Nature* **629**, 769–772 (2024).
- [124] S. Chatterjee and G. Hazra, *The Astrophysical Journal Letters* **997**, L27 (2026).
- [125] J. Pelt and O. Kärner, *On the variability of total solar irradiance* (2012), arXiv:1209.0322 [astro-ph.SR].
- [126] M. Dikpati, G. de Toma, and P. A. Gilman, *The Astrophysical Journal* **675**, 920 (2008).
- [127] V. D. Rusov, D. A. Litvinov, E. P. Linnik, V. N. Vaschenko, T. N. Zelentsova, M. E. Beglaryan, V. A. Tarasov, S. A. Chernegenko, V. P. Smolyar, P. O. Molchinikolov, K. K. Merkotan, and P. E. Kavatskyy, *Journal of Modern Physics* **04**, 528–550 (2013).
- [128] World Data Centre of Geomagnetism (Edinburgh), *Worldwide Observatory Annual Means* (2025).
- [129] N. S. Sidorenkov, *Odessa Astronomical Publications* **29**, 196–199 (2016).
- [130] N. S. Sidorenkov, *The Interaction between Earth’s Rotation and Geophysical Processes*, 1st ed. (Wiley, 2009).
- [131] International Earth Rotation and Reference Systems Service, *Earth orientation data* (2025).
- [132] NOAA Physical Sciences Laboratory, *Pacific Decadal Oscillation (PDO)* (2025).
- [133] NOAA Physical Sciences Laboratory, *AMO (Atlantic Multidecadal Oscillation) Index* (2023).
- [134] D. P. Chambers, M. A. Merrifield, and R. S. Nerem, *Geophysical Research Letters* **39**, 2012GL052885 (2012).
- [135] C. K. Folland, O. Boucher, A. Colman, and D. E. Parker, *Science Advances* **4**, eaao5297 (2018).
- [136] S. Takekawa, T. Oka, Y. Iwata, S. Tsujimoto, and M. Nomura, *The Astrophysical Journal* **871**, L1 (2019).